POLYOXOMETALATES

Open Access
REVIEW ARTICLE

Recent progress in the development of MOFs/POMOFs for light-mediated C–H bond activation

Yanjie Lv[1], Xinyu Zhao[1], Jing Sun[1] ✉, Wenxi Zhang[1], Xiao Li[1] ✉, and Zhongmin Su[1,2] ✉

[1] *School of Chemical and Environmental Engineering, Jilin Provincial Science and Technology Innovation Centre of Optical Materials and Chemistry, Jilin Provincial International Joint Research Center of Photo-functional Materials and Chemistry, Changchun University of Science and Technology, Changchun 130022, China*

[2] *State Key Laboratory of Supramolecular Structure and Materials, Institute of Theoretical Chemistry, College of Chemistry, Jilin University, Changchun 130021, China*

Cite This: *Polyoxometalates*, **2026**, *5*, 9140138

Read Online

ABSTRACT: The activation of inert C–H bonds under mild conditions with high selectivity remains a central challenge in catalysis. Metal–organic frameworks (MOFs) and polyoxometalate-based MOFs (POMOFs) offer atomically precise, tunable structures that integrate light absorption, charge separation, and catalytic sites. This review systematically summarizes recent progress in the development of MOFs/POMOFs for light-mediated C–H bond activation over the past decade. We discuss design strategies for active sites, including metal nodes, functionalized ligands, guest encapsulation, defect engineering, and single-site regulation. The synergistic role of POMs as electron sponges in promoting charge separation and modulating reactive oxygen species ($\cdot O_2^-$, $^1O_2$, and ·OH) pathways is discussed. Structure–activity relationships governing the activation of aromatic, benzylic, allylic, and aliphatic C–H bonds are discussed. Finally, perspectives on operando characterization, precision synthesis, green manufacturing, and AI-assisted design are provided to guide the development of next-generation photocatalysts.

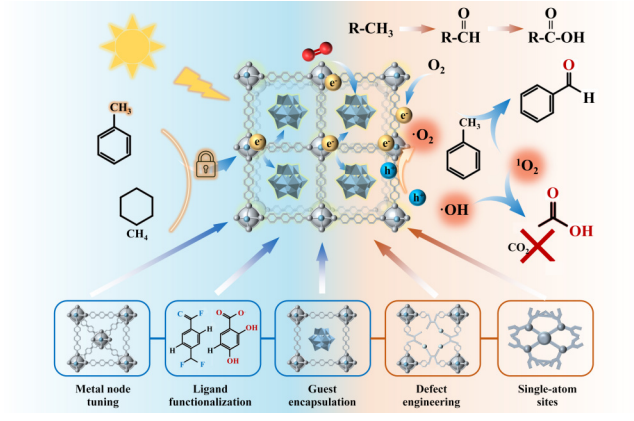

KEYWORDS: metal–organic frameworks (MOFs), polyoxometalate-based MOFs (POMOFs), photocatalysis, C–H bond activation

1 Introduction

The direct functionalization of inert C–H bonds is regarded as the Holy Grail of organic synthetic chemistry. If achieved with high efficiency and selectivity, this seemingly simple chemical bond transformation could provide a green path for directly obtaining high-value chemicals, such as alcohols, aldehydes, ketones, and acids, for use in the fields of medicine, pesticides, fine chemicals, and polymer materials. For example, according to industry statistics [1, 2], the demand for benzaldehyde increases 7% annually, and more than 50% of the market involves high-purity and chlorine-free products. The direct oxidation of C–H bonds would significantly shorten synthetic routes, enhance economic efficiency and environmental friendliness, and fundamentally drive the transformation of the organic synthesis field [3–5]. However, there remain significant obstacles, mainly due to the core contradiction of the universality and chemical inertness of C–H bonds [6–8]. The dissociation energy of the C(sp^3)–H bond is approximately 440 kJ/mol, which is a very high energy barrier to overcome [9, 10]. From a kinetic perspective, the weak polarity and high directionality of C–H bonds result in a low probability of orbital overlap between the substrate molecules and the active sites on a catalyst surface. Furthermore, the oxidation products are often prone to excessive oxidation as they are highly active [11–13]. Taking the selective oxidation of toluene as a representative example, the reactivity of the target product (benzaldehyde) is much higher than that of toluene. Once formed, benzaldehyde will rapidly further oxidize to benzoic acid and even mineralize into CO_2. Therefore, the synthesis of benzaldehyde with high selectivity under mild conditions remains an important challenge [14–17].

This activity–selectivity trade-off between activating inert C–H bonds and avoiding the overoxidation of labile products is the main scientific challenge. For over a century, chemical industries have used the side-chain chlorination hydrolysis of toluene oxidation to

Received: March 26, 2026; **Revised:** May 12, 2026
Accepted: May 27, 2026

✉Address correspondence to Jing Sun, sj-cust@126.com; Xiao Li, lix@cust.edu.cn; Zhongmin Su, zmsu@nenu.edu.cn

https://doi.org/10.26599/POM.2026.9140138

circumvent selectivity problems. However, this process is lengthy and generates a large amount of chlorine-containing waste, and meeting the strict chlorine-free product requirements of the food and medical fields is a challenge [18]. Moreover, although traditional volumetric oxidants such as $KMnO_4$ and CrO_3 have strong conversion capabilities, they are being gradually marginalized owing to their high toxicity, strong corrosiveness, and environmental risks as green synthesis becomes more popular [19–23]. Therefore, the development of strategies for efficiently activating inert C–H bonds under mild conditions and precisely controlling the reaction process to avoid excessive oxidation is a core challenge in contemporary catalytic chemistry, and a key path toward sustainable chemical synthesis.

Emerging photocatalytic technologies provide a new perspective for addressing these challenges [24]. Unlike traditional thermal catalysis relying on high temperature and pressure, some photocatalysts can directly capture solar energy and generate highly active species (such as photogenerated holes/electrons, and reactive oxygen species (ROS) generated by O_2 or H_2O) under normal temperature and pressure. Such photocatalysts can achieve the cleavage or isomerization of inert C–H bonds and initiate subsequent functionalization reactions [25–32]. Traditional photocatalysts, such as noble-metal complexes and inorganic semiconductors, exhibit significant limitations in practical applications. Although noble-metal complexes (such as Ru and Ir complexes) have high quantum efficiency and clear photophysical properties, they exhibit short excited-state lifetimes and rely on molecular diffusion and substrate collisions, which limit their catalytic efficiency [33–35]. Furthermore, the use of scarce rare-earth metals makes these catalysts expensive, and they are difficult to recycle to recover the valuable metals [36, 37]. Traditional inorganic semiconductors (such as TiO_2, CdS, and Bi_2WO_6) also exhibit limitations, such as severe photogenerated carrier recombination and inhomogeneous distribution of surface-active sites [38–41]. Furthermore, it is difficult to achieve atomic-level control of these semiconductors, thereby hindering an in-depth understanding of the catalytic mechanism and efficient performance optimization. Therefore, developing green photocatalysts that are both highly engineered and economically viable is the key to achieving efficient C–H bond functionalization under mild conditions [42].

The emergence of metal–organic frameworks (MOFs) brought about a structural revolution in photocatalysis [43]. MOFs can incorporate homogeneous catalytic units with well-defined structures (such as metal porphyrins [44], metal complexes [45], and metal oxygen clusters [46]) into a periodically extended framework through coordination bonds, ingeniously integrating the advantages of homogeneous and heterogeneous catalysis. The clear structure and controllable active sites of MOFs provided innovative strategies for catalyst design [47–49]. Furthermore, the insolubility, extremely high specific surface area (usually exceeding 1000 m^2/g), and tunable pore structures of MOFs enable easy recyclability, high substrate enrichment capacity, and size and shape selectivity, providing a unique confined environment that ensures stable intermediates and substrate recognition [50–52].

Polyoxometalates (POMs) are a class of atomically precise inorganic metal–oxygen clusters with excellent redox activity and reversible multi-electron storage capacity. POMs are described as electronic sponges because they can simultaneously and continuously accept and release electrons without destroying the structure [53–58]. However, POMs are easily soluble in polar solvents and exhibit low specific surface areas, which limit their application in heterogeneous catalysis [59, 60]. Encapsulating POMs within the regular pores of MOFs or constructing POM-based MOFs (POMOFs) using POMs as one of the raw materials through a one-pot method has become research priorities in recent years [61–64]. POMOFs address the problem of POM recovery while providing a novel cooperative catalysis platform. The MOF pores enrich the substrate and stabilize the intermediate, while the photosensitizing framework efficiently injects photogenerated electrons into the POMs. The POMs act as an electron sponge, further transferring electrons to O_2 or the substrate, thereby significantly promoting charge separation and subsequent oxidation reactions [65–70]. This multilevel structural design—from the molecule to framework scale—has opened up unprecedented pathways for developing high-performance photocatalysts (Fig. 1).

Compared with conventional photocatalysts, such as noble-metal complexes (e.g., Ru/Ir) and inorganic semiconductors (e.g., TiO_2 and CdS), MOFs and POMOFs offer several unique advantages. First, their atomically precise and periodically extended structures enable the rational integration of photosensitizers, catalytic centers, and substrate recognition sites within a single framework, bridging homogeneous and heterogeneous catalysis. Second, the tunable pore environment (size, shape, and hydrophobicity) provides confinement effects that stabilize reactive intermediates, enhance substrate enrichment, and provide size/shape selectivity features that are not accessible using traditional semiconductors. Third, the modular MOF structure enables post-synthetic modification and defect engineering to fine-tune electronic and catalytic properties. The incorporation of POMs as electronic sponges further imparts reversible multielectron storage and ultrafast charge separation, overcoming the severe carrier recombination that limits the performance of most inorganic photocatalysts. These combined advantages position MOFs and POMOFs as next-generation platforms for selective C–H bond activation under mild conditions.

This review aimed to systematically summarize the state-of-the-art progress in the development of MOF and POMOF materials for light-mediated C–H bond activation over the past decade, focusing on two core issues. First, material structures are precisely designed at the atomic level—including the selection of metal nodes, functionalization of organic ligands, encapsulation of guests, and interface construction—to precisely control the behavior of photogenerated charges and reactive oxygen species (ROS), as well as the activation pathways of C–H bonds. Second, the mechanism by which these design strategies translate into excellent activity and selectivity for specific reactions is systematically investigated. Through in-depth analysis and discussion of the mechanisms, we aimed to clarify the structure–activity relationship of MOF/POMOF catalysts and provide guidance for future catalyst design. This review demonstrates the advantages of MOFs/POMOFs in generating free radicals to activate C–H bonds and evaluates their use as a new strategy for synthesizing high-value chemicals through photocatalysis.

2 Design and synthesis of MOF/POMOF photocatalysts

The main advantage of MOFs/POMOFs is their highly designable structure [71–73]. The final performance of the catalyst depends on

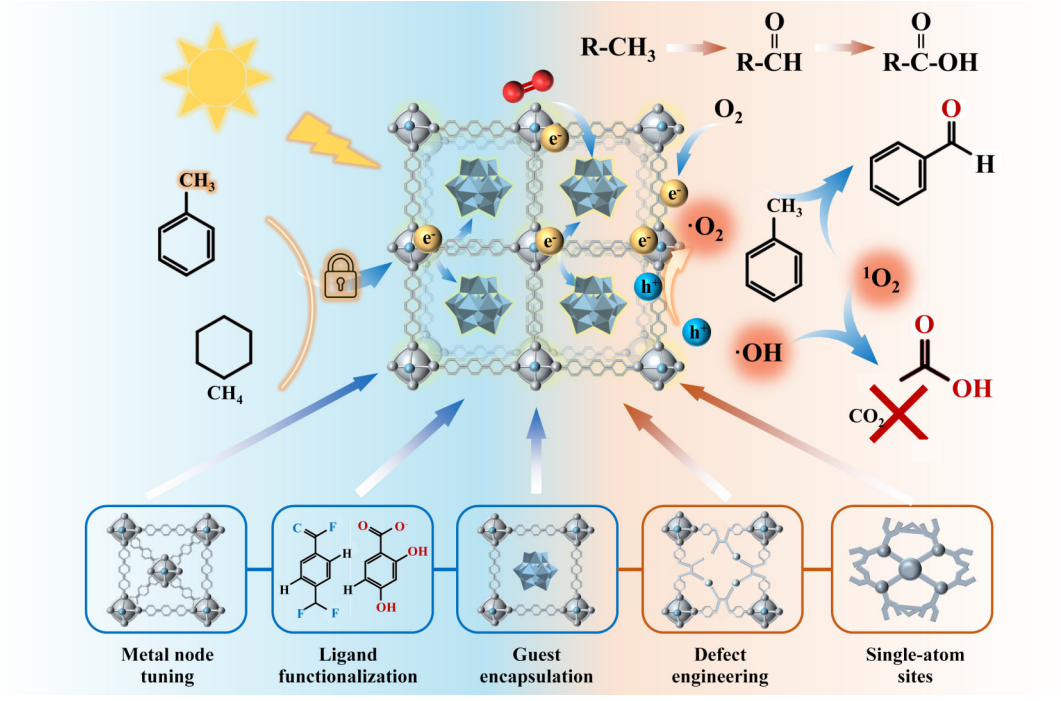

Figure 1 Schematic diagram of MOFs/POMOFs for photocatalytic C–H oxidation.

the appropriate selection and combination of photosensitive and catalytic centers, and pore environments to achieve the synergistic effects of electrons and spatial confinement [74–76].

2.1 Photocatalytic active sites in MOFs

The periodic structure of MOFs enables the precise positioning of different photocatalytic functional units at specific locations in three-dimensional (3D) space. These units can be derived from inorganic metal nodes, organic ligands, or guest molecules encapsulated in pores [77].

2.1.1 Metal–oxygen cluster nodes

The secondary building units of MOFs can often serve as catalytic centers [78]. Metal–oxygen clusters containing Fe, Ce, Zr, and Ti can be regarded as independent semiconductor quantum dots. They are excited indirectly via the antenna effect of organic ligands, resulting in ligand-to-metal charge transfer (LMCT) [79–83]. For instance, although the Zr–O clusters in Fe–UiO-66 do not absorb visible light, the ligands of amino benzoic acid can absorb visible light and inject electrons into the Zr oxygen clusters, thereby activating adsorbed O_2 or H_2O to achieve the efficient photocatalytic oxidation of C–H bonds (Fig. 2(a)) [84]. Notably, this LMCT process enables Zr–O clusters to achieve visible light activity, demonstrating the valuable effect of ligand nodes. Metal nodes may also possess unique chemical properties beyond those of traditional semiconductors [85]. For example, bimetallic Ce–O–Ce units in the Ce–AQ (anthraquinone) structure directly undergo LMCT under light irradiation, generating highly active bridging oxygen radicals that directly capture the hydrogen atoms of cyclohexane, achieving a selectivity of up to 98% for cyclohexanone (Figs. 2(b) and 2(c)) [86]. The mechanism by which metal–oxygen clusters directly participate in hydrogen atom transfer (HAT) is fundamentally different from the traditional pathway that relies on ROS for indirect oxidation. Hence, it demonstrates a new paradigm where metal nodes act as reaction centers [87]. Similarly, nodes containing Cl^- (such as the Ce–Cl units in the Ce-**MV**$^+$ structure) can generate highly active chlorine radicals in situ through LMCT, enabling HAT activation of inert substrates like cyclohexane, providing a new pathway for C–H bond oxidation (Fig. 2(d)) [88].

2.1.2 Functionalized organic ligands

The organic ligands that serve as the structural framework of MOFs can also act as photocatalytic centers. Through ingenious ligand design, the functions of light capture, energy transfer, and catalysis can be integrated to form a multifunctional cooperative catalytic system [89–91].

2.1.2.1 Photosensitive ligands

The inclusion of classical photosensitizer molecules directly used as ligands is the most intuitive strategy. For example, the porphyrin ligand in PCN-222(H_2), the pyrene ligand in NU-1000, and the 1,4-bis(phenylethynyl)benzene ligand in SIU-100 are excellent light-absorption antennas, which can efficiently transfer light energy to the entire framework. Interestingly, the close stacking and π–π interactions between the ligands in these MOFs result in distinct excited-state behavior compared to that of free ligands. It was shown that ligands can form migratable singlet excitons (mobile singlet electron–hole pairs) in NU-1000, preventing the generation of singlet oxygen and ensuring that superoxide radicals are the main ROS type [92, 93]. This demonstrates that the MOF structure can fundamentally alter the relaxation pathways of the excited states of photosensitizers, providing new strategies for regulating the types of ROS produced (Fig. 3).

2.1.2.2 D–A type ligands

Integrating electron donors (D) and acceptors (A) into the same ligand or constructing D–A-type MOFs through a mixed-ligand strategy is an effective method for promoting charge separation [94]. It was demonstrated that JNU-204 (a D–A–D type pyrazole-benzothiadiazole-pyrazole ligand) [95] and Zr-NDI-H_2DPBP (a naphthalene diamide ligand acceptor and a porphyrin ligand

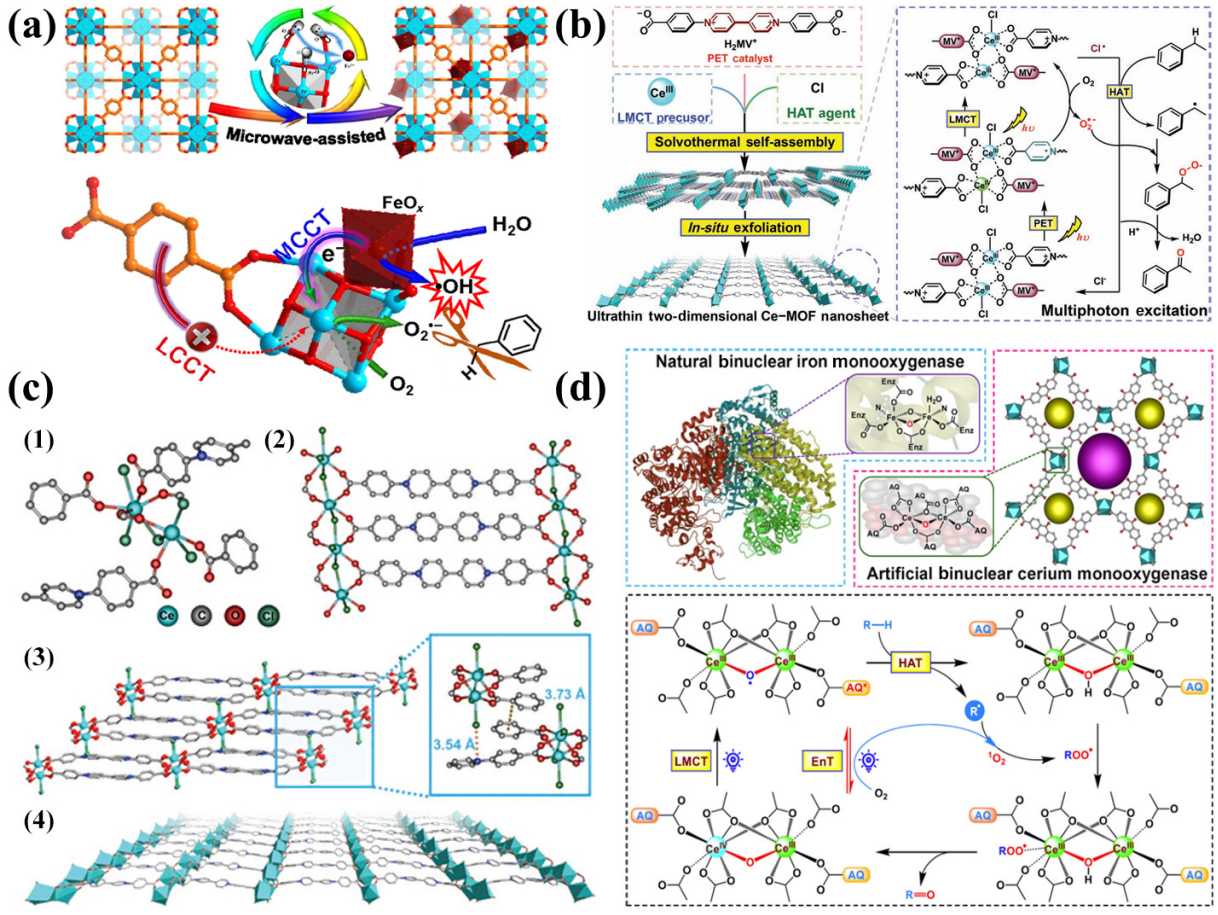

Figure 2 (a) Schematic illustration showing the grafting FeO_x onto the Zr-oxo cluster by coordination interaction, affording Fe-UiO-66 and the conversion of H_2O to ·OH by visible-light-driven metal-to-cluster charge transfer (MCCT) process, which is accomplished by the holes on FeO_x, upon electron transfer from FeO_x to Zr-oxo cluster, and the conversion of O_2 to $\cdot O_2^-$ based on the accepted electrons on the Zr-oxo clusters. In contrast, the LCCT process does not occur under visible light irradiation. Adapted with permission from Ref. [84], © American Chemical Society 2019. (b) Schematic illustration of the building blocks of the layered metal–organic framework Ce-MV^+, and the development to produce 2D MOF monolayer nanosheets via *in situ* exfoliation approach. The multiphoton excitation concepts trigger including the photoinduced electron transfer (PET) of initial excitation, the LMCT excitation on the cerium center, and the final HAT activation of inert $C(sp^3)$–H bonds step-by-step, and environmentally benign oxygenation reactions with active oxygen species. (c) (1) The Ce_2 secondary building unit of MOF Ce-MV^+. (2) Coordination environments of cerium ions and the one-dimensional (1D) Ce chains in MOF Ce-MV^+ along the a-direction. (3) Single-crystal structures of the 3D layered Ce-MV^+, detail view showed the π–π and electrostatic interactions between the adjacent layer. (4) The ultrathin 2D monolayer Ce-MV^+ nanosheet. Adapted with permission from Ref. [86], © Wiley-VCH GmbH 2023. (d) Natural binuclear iron monooxygenase (PDB code: 64WX2). MOF-based artificial binuclear cerium monooxygenase. The photoexcitation of MOF-based artificial monooxygenase triggers the hydrogen atom transfer process for the selective oxidation of inert $C(sp^3)$–H bonds, including the energy transfer and ligand-to-metal charge transfer for the formation of singlet oxygen and oxygen bridge radicals, respectively. Adapted with permission from Ref. [88], © American Chemical Society 2022.

donor) [96] generated long-lived charge-separated states under light irradiation, thereby prolonging the lifetime of photogenerated carriers to provide sufficient time for surface reactions, and significantly enhancing photocatalytic oxidation activity (Fig. 4).

In summary, functionalized organic ligands in MOFs enable three distinct photocatalysis strategies: (i) Photosensitive ligands (e.g., porphyrin and pyrene) serve as light-harvesting antennas; (ii) D–A-type ligands (e.g., Naphthalene Diimide-porphyrin) facilitate intramolecular charge separation; and (iii) HAT-active ligands (e.g., benzophenone and fluorenone) directly abstract hydrogen atoms from substrates. These ligand-level designs collectively expand the photocatalytic versatility of MOFs beyond conventional metal-node-centered mechanisms.

2.1.2.3 Ligands with HAT functionality

Directly fixing a HAT catalyst onto a ligand enables the close activation of the substrate, which is an important step in mimicking enzyme catalysis [97]. For example, carmine Y dye was anchored onto the Zr clusters in eosin Y-decorated MOF-808 (Fig. 5(a)) [98]. After absorbing light energy, the dye activated benzyl alcohol via HAT, and the adjacent Zr unsaturated sites preferentially coordinated benzyl alcohol rather than the benzaldehyde product, achieving high selectivity for alcohol oxidation. The key to this design lies in the dual roles of the MOF as a light-sensitizer carrier and a substrate-recognition receptor, demonstrating the broad potential of host–guest synergy. Furthermore, it was demonstrated that the 9-fluorenone ligand in the Zn-OFDC MOF forms hydrogen bonds with 2,2,2-trichloroethanol through pore confinement, generating alkoxyl radicals via proton-coupled electron transfer, which served as HAT reagents to achieve C–H functionalization of aldehydes and ethers (Fig. 5(b)) [99].

2.1.3 Molecular encapsulation

The pore channels of MOFs can serve as nanoreactors,

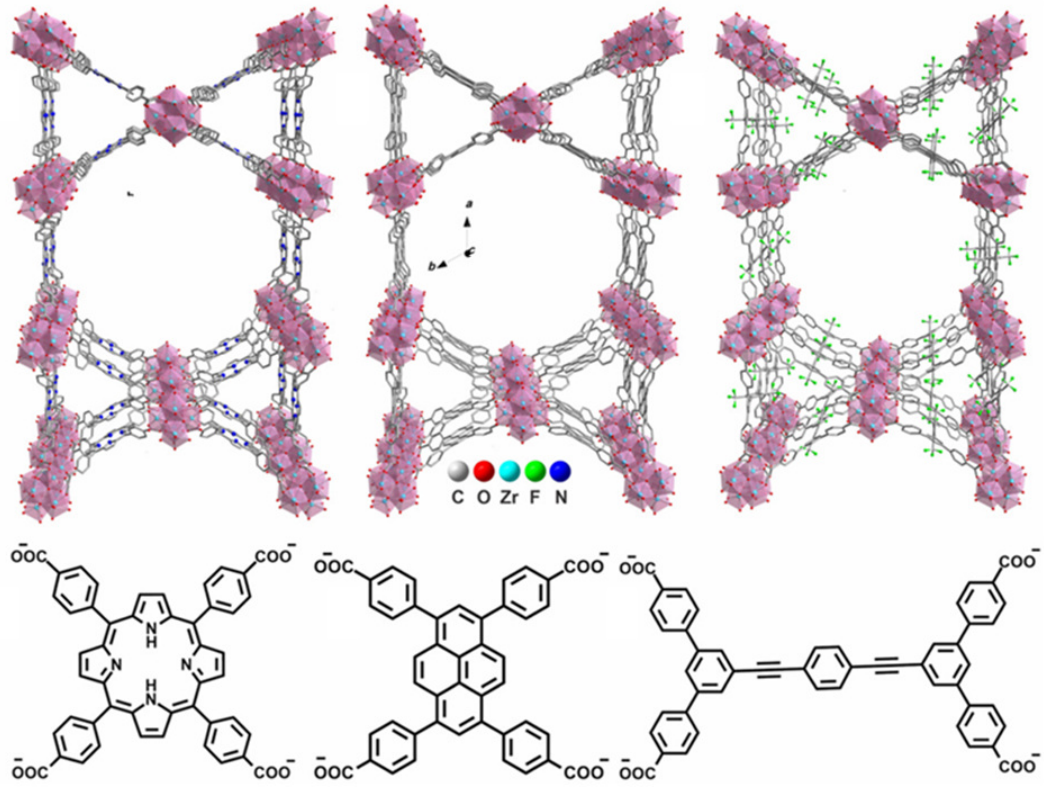

Figure 3 Structurally comparable *csq/xly* MOFs (referring to the underlying framework topology types) PCN-222(H_2), NU-1000, and SIU-100 constructed from electronically diverse linkers TCPP(H_2)$^{4-}$, TBAPy^{4-}, and PEPF^{4-}, respectively; H atoms were omitted for clarity. Adapted with permission from Ref. [93], © American Chemical Society 2025.

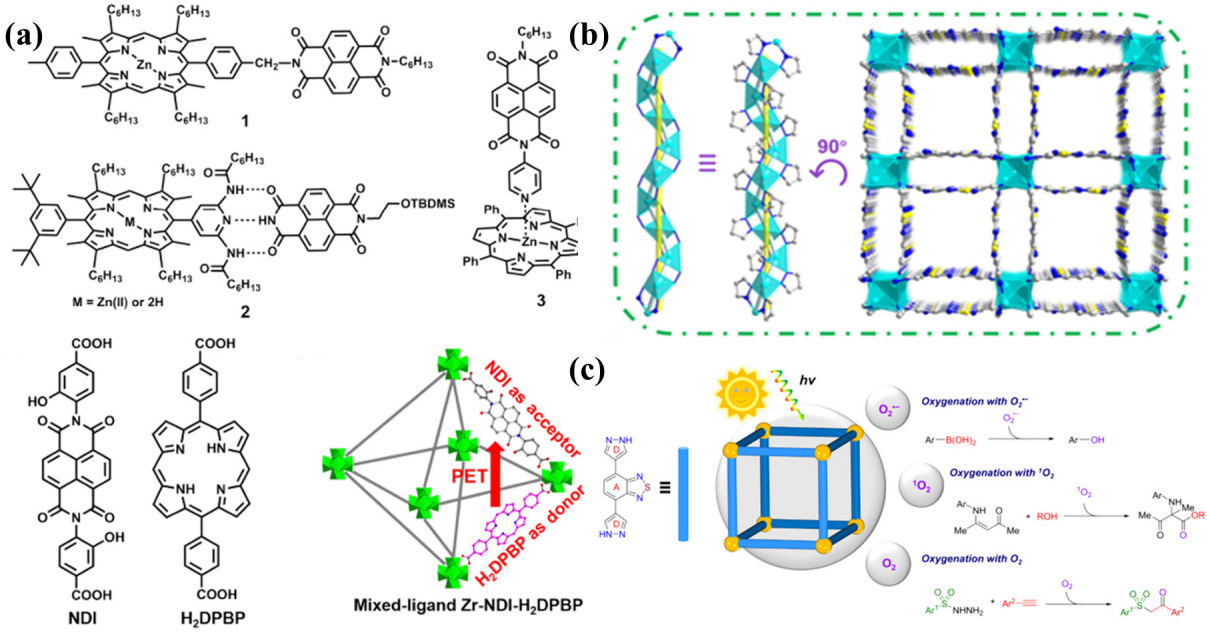

Figure 4 (a) Three representative PET models 1–3 based on covalent or non-covalent systems using porphyrins as donors and NDI as Chemical structures of the NDI and H_2DPBP ligands. The targeted PET model of mixed-ligand MOF Zr-NDI-H_2DPBP based on donor H_2DPBP and acceptor NDI used in this work. Adapted with permission from Ref. [95], © American Chemical Society 2023. (b) Crystal structure of JNU-204. ZnN_4 clusters (cyan tetrahedra) are connected through edge-sharing pyrazoles to form helical rod SBUs, further cross-linked through PBT linkers into a 3D framework with square channels along the [001] direction (Zn, sky blue; O, red; C, gray; N, blue; H atoms are omitted for clarity). (c) Schematic illustration of JNU-204 as photocatalyst for aerobic oxygenation under visible-light irradiation. Adapted with permission from Ref. [96], © American Chemical Society 2021.

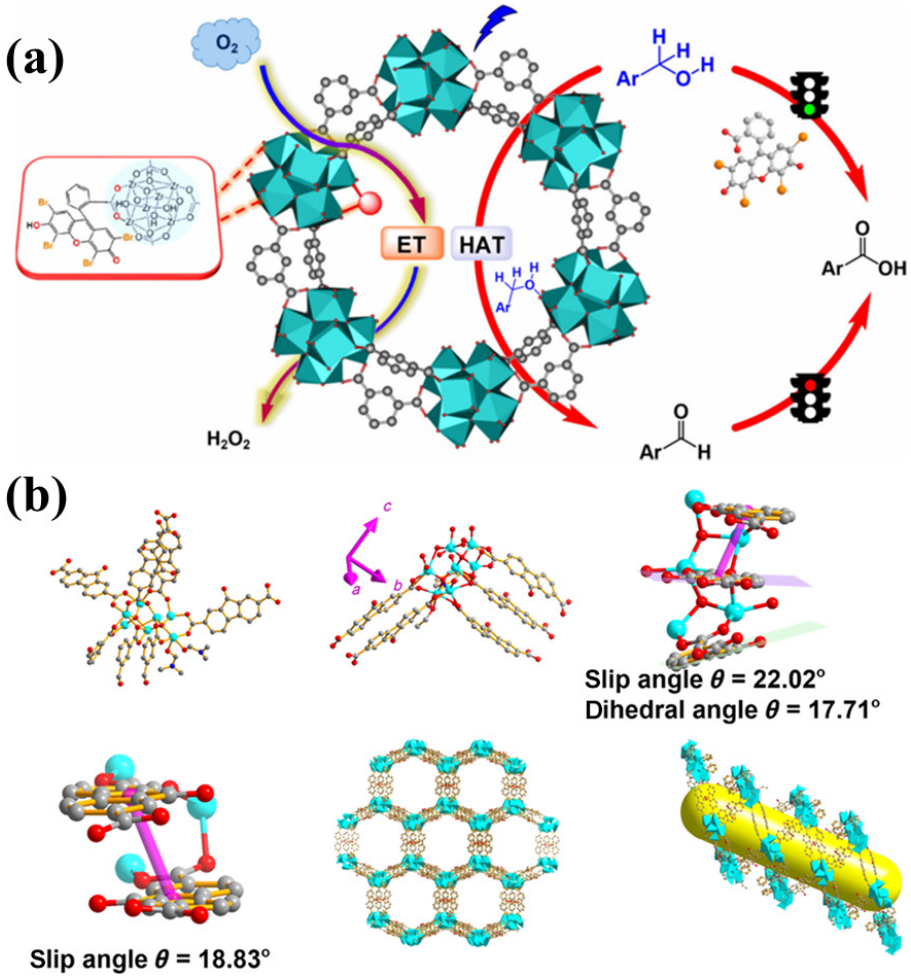

Figure 5 (a) Schematic of the eosin Y-decorated MOF-808 for the selective photocatalytic oxidation of benzylic C(sp^3)–H bonds via HAT events and electron transfer process. Adapted with permission from Ref. [98], © American Chemical Society 2024. (b) Coordination model of Zn-OFDC, arrangement of OFDCs, slip angle and dihedral angle for one J-aggregation, slip angle for the other J-aggregation, hexagonal channels in Zn-OFDC, and spiral structure of the hexagonal channels in Zn-OFDC. Adapted with permission from Ref. [99], © American Chemical Society 2021.

encapsulating functionalized guest molecules to construct a cooperative host–guest catalytic system. This is advantageous because the functionality of the guest molecules can complement and enhance that of the framework. The impregnation of organic dye EY@MOF-808 into a MOF results in the homogenization of the dye, while the MOF pore channels regulate the reaction selectivity. Recent research demonstrated the encapsulation of a fluorescent probe targeting cancer-cell membrane receptors in PCN-Ru, achieving the precise photooxidation treatment of phospholipids in tumor-cell membranes (Fig. 6) [100, 101]. This cross-disciplinary application demonstrates the broad potential of MOF host–guest chemistry in the field of biomedicine and the viability of extending photocatalytic oxidation from organic synthesis to life sciences, providing new tools for precise treatments [102].

2.1.4 Defect engineering and single-site regulation

In addition to the three strategies described above, defect engineering and single-site regulation have emerged as powerful tools for optimizing MOF photocatalysts. Defect engineering intentionally introduces missing linkers or metal node vacancies into the MOF, thereby generating unsaturated coordination sites and structural distortions that modulate band structures, enhance substrate adsorption, and expose more active centers. For example, in Def-CuCN/NU (Section 3.4.2), mesoporous defects promote methane adsorption and rapid methanol desorption, suppressing overoxidation [103]. Single-site regulation refers to the precise anchoring of isolated metal atoms (e.g., Cu, Fe, and Ni) at MOF nodes or within pores, maximizing active-site utilization and enabling the precise control over reaction pathways. In the Def-CuCN/NU catalyst, the Cu single-atom sites steer O_2 activation toward hydroperoxyl radical (·OOH) rather than hydroxyl radicals (·OH), dramatically improving the selectivity of methane oxidation [103]. These two strategies complement metal nodes, functionalized ligands, and guest encapsulation, collectively enriching the design toolbox for MOF/POMOF photocatalysts.

The above three strategies for designing active sites in MOFs (metal nodes, functionalized ligands, and guest encapsulation) have made significant progress, but remaining limitations include insufficient charge-separation efficiency and multi-electron transfer capability. In particular, for highly inert C–H bond oxidation reactions that require multiple electrons, a single MOF often fails to simultaneously provide efficient sensitization, rapid electron transfer, and stable active sites. Therefore, POMs have attracted attention as a class of inorganic metal–oxygen clusters with excellent redox activity and reversible multielectron storage

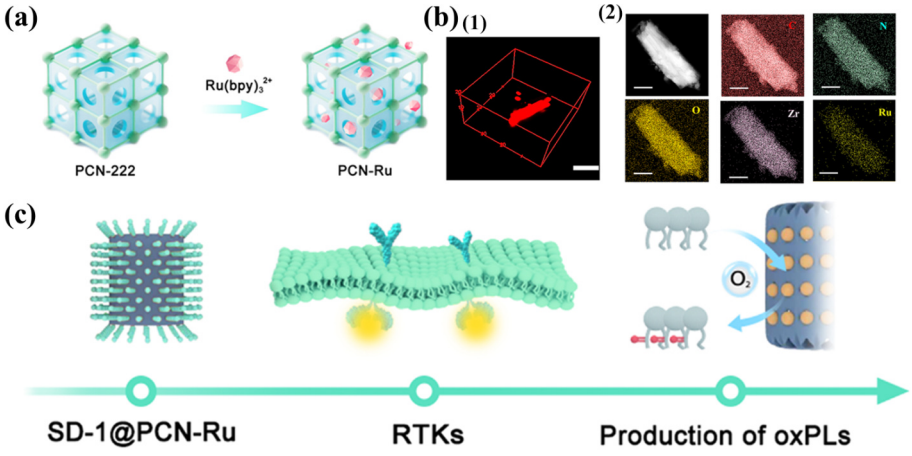

Figure 6 (a) Schematic diagram of the synthesis of PCN-Ru. (b) (1) Fluorescence emission of Ru complexes in PCN-Ru (scale bar: 200 nm). (2) TEM images and elemental maps of PCN-Ru (scalebar: 300 nm). (c) The process of fluorescence emission and oxidative activation in SD-1@PCN-Ru. Adapted with permission from Ref. [101], © Wiley-VCH GmbH 2026.

capacity. Introducing POMs into MOF systems to construct POMOF composite materials takes advantage of the electronic sponge property of POMs to promote photogenerated charge separation while expanding the light-absorption range and providing additional HAT active centers, thereby achieving the collaborative catalysis of the MOF and POM guest. The following sections systematically discuss POMOF design strategies and their synergistic effects in photocatalytic C–H activation.

2.2 POMOFs: Integrating the advantages of POMs and MOFs

POMOFs are not a simple physical mixture of POMs and MOFs but a new hybrid material constructed through the interaction between the host and guest, with strong electronic coupling effects. Unlike the physical encapsulation of other molecules (such as organic dyes like Eosin Y (EY)), as described in Section 2.1.3, POMs in POMOFs typically exhibit stronger electronic coupling with the MOF. Unlike the post-synthesis impregnation methods commonly used to insert various molecules into MOFs, POMOFs (such as CuW_{10}-TIPA and NiW_{12}-TPT) can be synthesized using one-pot self-assembly or in situ templating methods to insert POMs into MOFs via covalent or strong hydrogen bonds. In terms of electronic coupling strength, many molecules interact with MOFs through van der Waals forces or weak coordination, resulting in a relatively slow photogenerated charge-transfer rate (approximately 10^8–10^9 s^{-1}). By contrast, in POMOFs, the lowest unoccupied molecular orbital (LUMO) levels of POMs are more compatible with the highest occupied molecular orbital (HOMO) levels of MOF ligands, enabling extremely fast (picosecond-scale) electron injection (~10^{11} s^{-1}). In terms of the synergistic mechanism, most guest molecules mainly act as additional photosensitizers or HAT reagents, whereas POMs simultaneously function as electron sponges, charge-separation centers, and oxidation-active sites, enabling multi-electron storage and controlled release. The synergistic effects of POMs manifest throughout the light absorption, charge separation, and surface reaction steps [104–106].

2.2.1 *Photocatalytic properties of POMs*

POMs play multiple roles in photocatalysis. As a photosensitizer, the decatungstate is a typical HAT photocatalyst, which is excited under ultraviolet light and directly captures hydrogen atoms from the substrate by generating an active W–O intermediate. This process has been widely applied in POMOF designs such as CuW_{10}-TIPA (Fig. 7(a)) [107] and CUST-906 (Fig. 7(b)) [108]. The electron-sponge functionality of POMs enables them to accept multiple electrons and maintain excellent stability in their reduced state. For instance, the reversible electronic capacity of a typical Keggin-type POM (such as $PW_{12}O_{40}^{3-}$) can reach 24 electrons, with a reduction potential range of −0.2 to −0.8 V (vs. NHE) [108]; transient absorption spectroscopy identified an electron injection rate from a light-excited MOF to a POM of ~ 10^{11} s^{-1} (i.e., reactions occurring within a few picoseconds). In MOF systems, POMs can act as efficient receptors for photogenerated electrons, inhibiting charge recombination in the framework [109]. The introduction of the $[H_2W_{12}O_{40}]^{6-}$ POM into NiW_{12}-TPT enabled the migration of photogenerated electrons from the $TPT^{+\cdot}$ ligand to the cluster, achieving continuous multi-step electron transfer and significantly prolonging the charge-separation state lifetime (Fig. 7(c)) [110].

2.2.2 *Design strategy for POMOFs*

When introducing POMs into MOFs, it is critical to achieve stable and orderly loading and ensure electronic communication between the two materials. The main strategies for achieving this include: (1) *in situ* templating; (2) post-synthesis impregnation; and (3) one-pot self-assembly.

In situ templating was performed using POM molecules larger than the MOF window as templates, which were encapsulated into the MOF pores during POMOF synthesis [111]. The POMs in the resulting POMOFs were firmly locked in the framework cage with excellent stability. Typical NENU series materials are highly ordered superstructures formed by encapsulating Keggin-type POMs into the pore cage of the HKUST-1 MOF (Figs. 8(a) and 8(b)).

In post-synthesis impregnation methods, large-window MOFs (such as MIL-101 and NU-1000) are first synthesized, and pre-synthesized POM molecules are impregnated into the MOF pores. This method requires a high degree of matching between the sizes of the POM molecules and MOF windows, but it is flexible and suitable for thermally sensitive POMs. The PW_{12}@NU-1000 POMOF was prepared using this method, and X-ray diffraction (XRD) and electron microscopy confirmed that the POM molecules were uniformly distributed in the mesoporous channels of the MOF (Fig. 8(c)) [112].

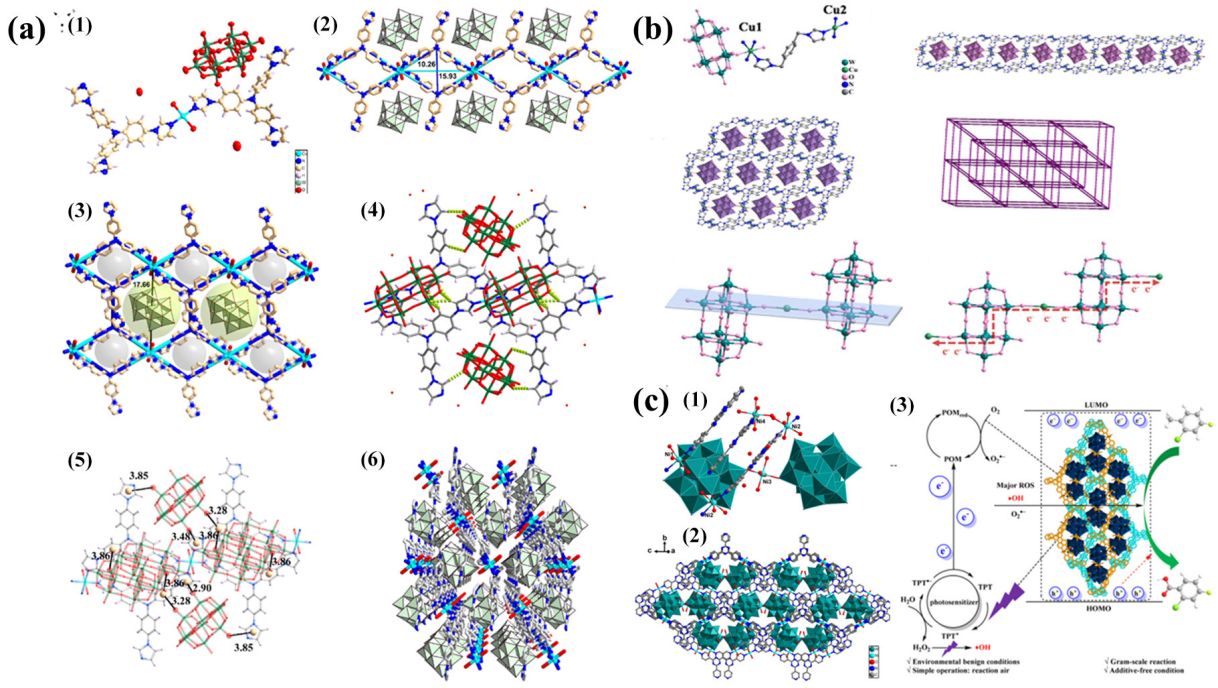

Figure 7 (a) (1) Unit cell of CuW_{10}-TIPA. (2) and (3) 2D layer of CuW_{10}-TIPA along the *b*-axis. (4) Hydrogen bonds between TIPA with $[W_{10}O_{32}]^{4-}$. (5) Anion···π interactions in CuW_{10}-TIPA between POM anion and faces of the TIPA rings. (6) 3D stacking diagram of CuW_{10}-TIPA. Adapted with permission from Ref. [107], © Elsevier Inc. 2024. (b) Asymmetric unit of CUST-906. Adapted with permission from Ref. [108], © Elsevier Inc. 2025. (c) (1) Coordination environment of Ni(II) ions in NiW_{12}-TPT. (2) 3D structure of NiW_{12}-TPT. (3) Design concept of NiW_{12}-TPT for the photocatalytic oxidation of hydrocarbons. Adapted with permission from Ref. [110], © The Royal Society of Chemistry 2025.

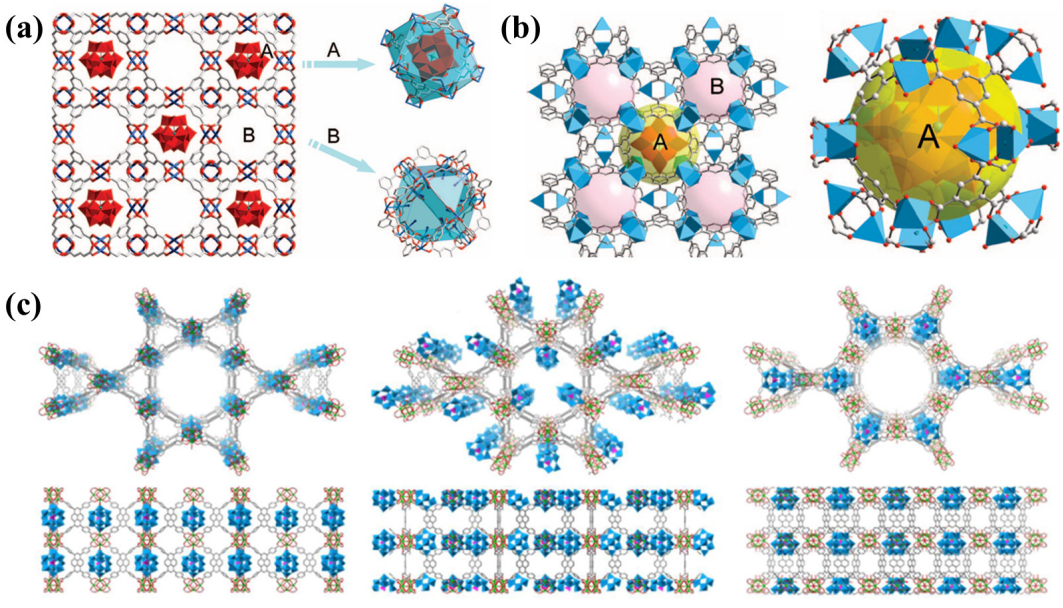

Figure 8 (a) View of a (001) sheet with two kinds of pores, A and B, in NENU-*n* (*n* = 1–6). The Cu-BTC framework and Keggin polyanions are represented by wireframe and polyhedral models. Blue, red, and gray represent Cu, O, and C, respectively. (b) Components of the crystal structures of NENU-*n* (*n* = 1–6): a cube of five truncated-octahedral cages sharing square faces; the pore A accommodating the Keggin polyanion, Cu_2-cluster (blue polyhedra), Keggin polyanion (red polyhedra), C (gray), and O (red). All H atoms and solvent molecules are omitted for clarity. Adapted with permission from Ref. [111], © American Chemical Society 2009. (c) Visual representations (top and side view) of the proposed structures for PW_{12}@NU-1000, where the POM is located inside the windows between the channels, in the hexagonal channels, or in the small triangular channels. DED mapping of PW_{12}@NU-1000 has led to the conclusion that is most representative of the material. Adapted with permission from Ref. [112], © American Chemical Society 2017.

In the one-pot self-assembly method, a mixture containing POMs, metal salts, and organic ligands is reacted, allowing the POMs to participate in the construction of the MOF or act as a template to induce the formation of a specific topological structure. CuW_{10}-TIPA and NiW_{12}-TPT POMOFs produced using one-pot methods, as confirmed by single-crystal XRD, exhibited covalent or strong hydrogen bond interactions between the POMs and the metal-ligand framework, with stronger electronic coupling and

more significant synergistic effects [107, 109].

2.2.3 *Synergistic effect of POMOFs in photocatalysis*

The catalytic performance of POMOFs far exceeds that of any single component. The synergistic effects are observed at multiple levels, such as the expansion of the light-absorption range and regulation of the energy band structure. The band gap of tetrabutylammonium decatungstate (TBADT) salt is 3.01 eV, limiting its response to the ultraviolet region [107]. When combined with the Cu-TIPA MOF to form the CuW_{10}-TIPA POMOF, the band gap decreased to 2.27 eV, and the light-absorption range significantly shifted to the visible region. This energy-band optimization stems from the electronic coupling between POMs and MOFs, enabling POMOFs to efficiently utilize visible light (Fig. 9(a)), while promoting charge separation and prolonging carrier lifetime. Analysis of the photoluminescence (PL) spectrum of NiW_{12}-TPT showed that the introduction of $[H_2W_{12}O_{40}]^{6-}$ led to a sharp decrease in PL intensity, indicating that it suppressed charge recombination [110]. The transient absorption spectrum further revealed that photogenerated electrons migrated from the ligand 2,4,6-tri(2-pyridyl)-s-triazine (TPT) to the POM cluster within picosecond timescales, forming a long-lived charge-separated state. The photocurrent response and electrochemical impedance spectroscopy analysis of CuW_{10}-TIPA also confirmed that the introduction of the POM significantly enhanced charge separation and interface transfer efficiency (Figs. 9(b)–9(d)). Integrating different reaction pathways achieved synergistic catalysis. Furthermore, a study of SiW_{12}@CuMOF-1 demonstrated that after light excitation, the Cu site undergoes LMCT to generate Cl· radicals for HAT, whereas the NAD^+ mimetic ligand generates $^1O_2$ and $\cdot O_2^-$ through energy and electron transfer, respectively [113]. The three active species, under the collaborative action of the Cu site, POM, and ligand, collaboratively achieve the efficient oxidation of 3,5-dibutylphenol. This design achieved the effective integration of multiple activation pathways by a single catalyst, demonstrating the great potential of the POMOF platform (Fig. 9(e)).

Notably, the specific structure of the incorporated POM significantly influences the charge-separation efficiency and ROS selectivity of a POMOF. Decatungstate ($[W_{10}O_{32}]^{4-}$) exhibits a relatively low reduction potential and is readily excited under ultraviolet (UV)/visible light to generate highly reactive W–O· species that directly abstract hydrogen atoms via HAT, favoring $\cdot O_2^-$ as the primary ROS. In MOF-confined systems, such as CuW_{10}-TIPA and CUST-906, decatungstate maintains its HAT-dominated pathway with fast (picosecond) electron injection. Keggin-type POMs (e.g., $[PW_{12}O_{40}]^{3-}$) possess moderate reduction potentials and large reversible electron capacity (up to 24 electrons), acting primarily as electron acceptors that promote charge separation. The ROS selectivity in Keggin-based POMOFs (e.g., PW_{12}@NU-1000) is more dependent on the MOF exciton behavior, often generating ROS mixtures (mainly $\cdot O_2^-$ with minor $^1O_2$). Wells–Dawson-type POMs (e.g., $[P_2W_{18}O_{62}]^{6-}$) have stronger oxidizing power and higher reduction potentials, yet few studies have investigated their confinement in MOFs. In Cu-P_2Mo_{18}, the Wells–Dawson POM cooperates with Cu sites to generate ·OH or t-BuO· radicals,

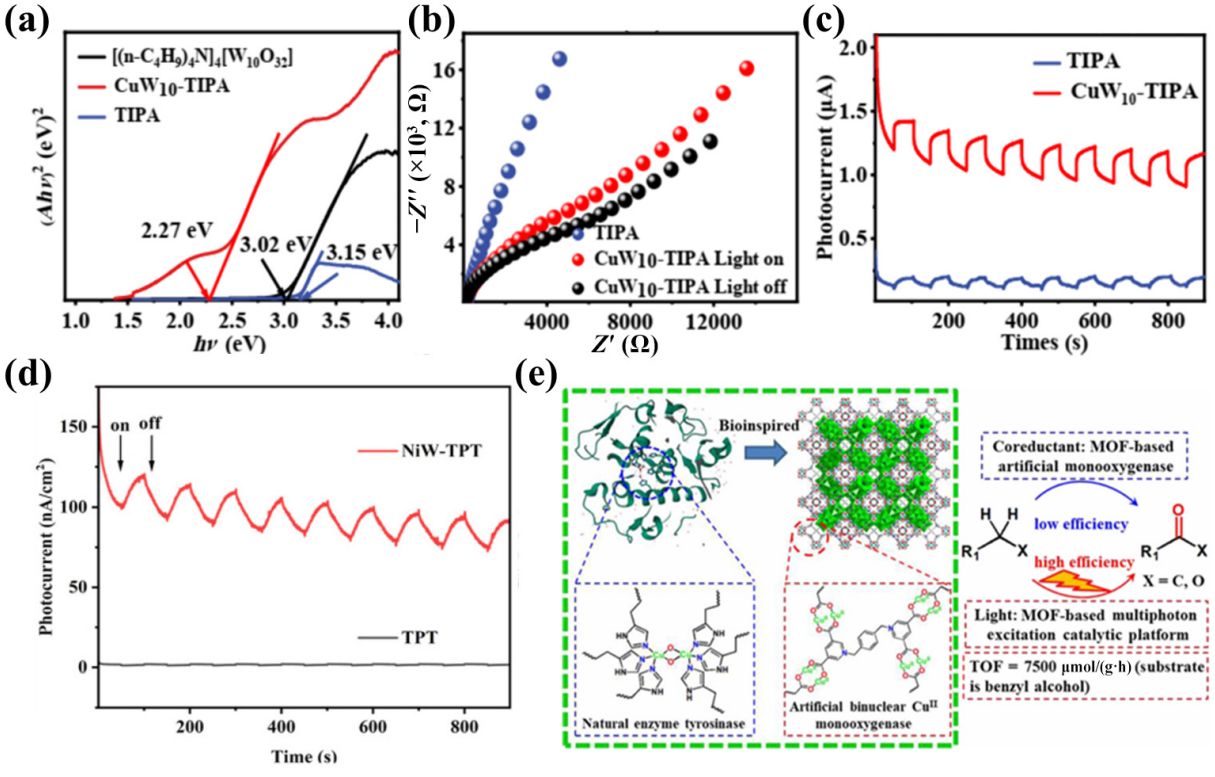

Figure 9 (a) Tauc plots of CuW_{10}-TIPA, TIPA and $[(n\text{-}C_4H_9)_4N]_4[W_{10}O_{32}]$. (b) EIS Nyquist plots of CuW_{10}-TIPA in 0.1 M Na_2SO_4 aqueous solution without bias versus Ag/AgCl electrode irradiated with 300 W xenon lamp light. (c) Transient photo current response of CuW_{10}-TIPA in 0.1 M Na_2SO_4 aqueous solution without bias vs. Ag/AgCl electrode irradiated with white light. Adapted with permission from Ref. [107], © Elsevier Inc. 2024. (d) Transient photocurrent response of TPT and NiW_{12}-TPT. Adapted with permission from Ref. [110], © The Royal Society of Chemistry 2025. (e) Schematic of the NAD^+ mimics incorporated copper-organic framework containing the binuclear copper catalytic sites and the embedded polyoxometalates and the exogenous chloride sources for the selective monooxygenation of substrates. Adapted with permission from Ref. [113], © American Chemical Society 2023.

achieving high selectivity for benzylic C–H oxidation. Overall, the charge-separation efficiency is governed by LUMO level matching between the POM and MOF linker, as well as the strong electronic coupling between the POM and metal nodes, whereas ROS selectivity is controlled by the reduction potential and excited-state reactivity of the POM. Systematic comparative studies using the same MOF host with different POM guests are still lacking and represent an important future research direction.

2.3 Mechanism of photogenerated electron separation and transport in MOFs/POMOFs

Understanding the generation, separation, and migration of charges in MOFs/POMOFs is the theoretical basis for rational photocatalyst design [114–116]. Efficient charge separation is a key prerequisite for photocatalytic C–H activation, as it directly determines the availability of photogenerated electrons and holes for subsequent surface reactions. Three primary charge-separation mechanisms are discussed here: (1) LMCT, (2) node-to-node charge transfer, and (3) POM-mediated charge separation, followed by the generation of ROS.

2.3.1 *Ligand–metal charge transfer*

Ligand–metal charge transfer is the most fundamental charge-separation mechanism in MOFs. After the ligand is excited by light, the photogenerated electrons can be injected from the LUMO of the ligand into the conduction band of the metal node, confining the electrons and holes to the metal and ligand, respectively [117]. In Fe-UiO-66, the amino benzoic acid ligand absorbs visible light and injects electrons into the Zr–O cluster, achieving efficient charge separation (Fig. 10(a)) [84]. Transient absorption spectroscopy indicated that this process occurs on the picosecond scale and is one of the fastest charge-separation pathways in MOF photocatalysis.

2.3.2 *Node-to-node charge transfer*

In multicomponent or multimetal MOFs, electrons can transfer between different metal nodes, enhancing the spatial separation of charge-separated states [118]. A density functional theory (DFT) study of the c-Ni_5-Co_4 catalyst showed that after light excitation, photogenerated electrons were transferred from the ligand of the Ni_5 cluster to the W–O framework of the Co_4-POM, while the holes were confined to the metal center of the Ni_5 cluster and the Co center of the Co_4-POM [119]. This charge separation enables the simultaneous progression of the reduction and oxidation half-reactions. The good agreement between theoretical calculations and experimental results indicated that DFT is a powerful tool for understanding the charge-transfer pathway at the atomic level (Figs. 10(b) and 10(d)).

2.3.3 *POM-mediated charge separation*

In POMOF systems, the POM often acts as an efficient electron acceptor, facilitating charge separation over a large spatial scale. In a representative system, pyrene ligands (TBAPy) are excited, and electrons are rapidly injected into adjacent PW_{12} clusters, thereby reducing the clusters, while the holes remain on the ligand [112]. Transient absorption spectroscopy indicated that electron injection occurs within a few picoseconds, and charge recombination is delayed to the nanosecond or even microsecond scale, indicating

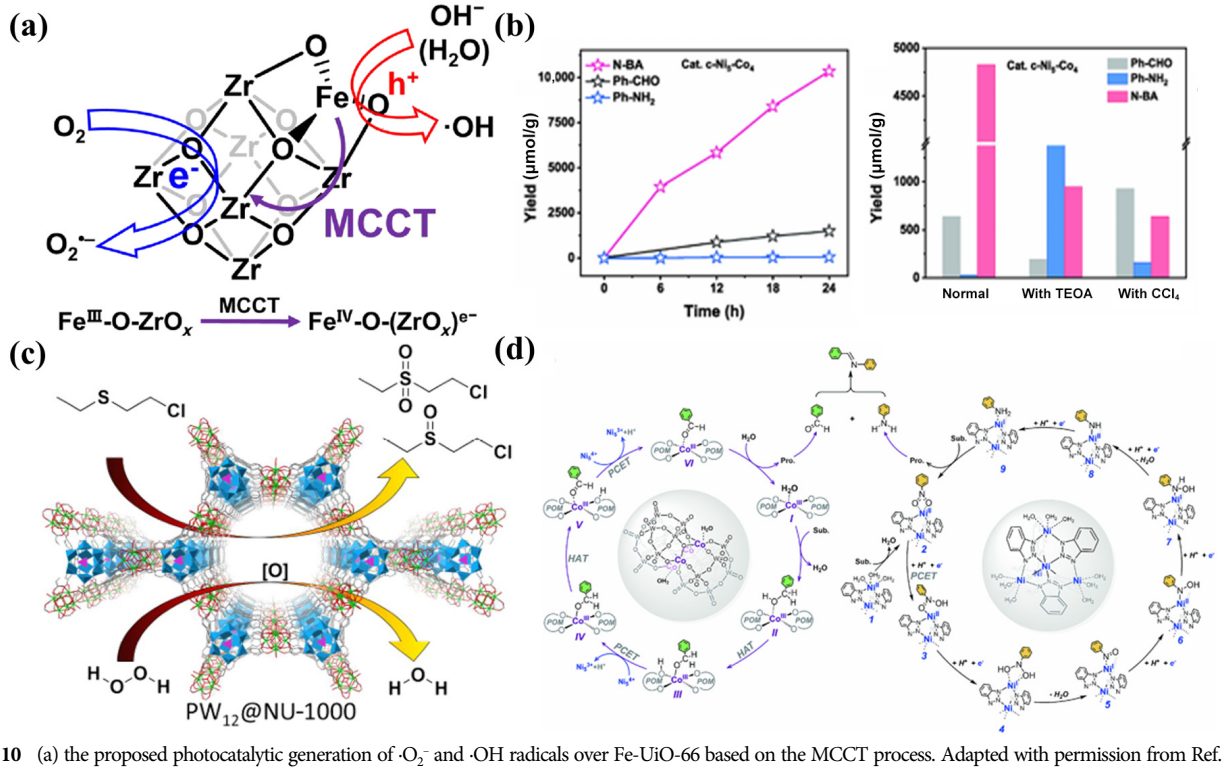

Figure 10 (a) the proposed photocatalytic generation of $\cdot O_2^-$ and ·OH radicals over Fe-UiO-66 based on the MCCT process. Adapted with permission from Ref. [84], © American Chemical Society 2019. (b) (1) Time-dependent yields of N-BA, Ph-CHO, and Ph-NH_2 catalyzed by c-Ni_5-Co_4. (2) Control experiments using different radical quenchers for the selective photocatalytic synthesis of Schiff base in a coupled system of Ph-CH_2OH and Ph-NO_2 over c-Ni_5-Co_4 under visible light illumination for 12 h. Adapted with permission from Ref. [117], © Science China Press 2024. (c) A channel-type POM@MOF (PW_{12}@NU-1000) was synthesized for the first time. The hybrid material shows stability and enhanced activity towards the oxidation of organosulfur with hydrogen peroxide. Adapted with permission from Ref. [112], © American Chemical Society 2017. (d) The proposed possible mechanism. Adapted with permission from Ref. [117], © Science China Press 2024.

efficient charge separation (Fig. 10(c)).

2.4 ROS generation

Molecular oxygen (O_2) is the ideal oxidant for photocatalytic C–H bond oxidation, as it is abundant, inexpensive, and environmentally friendly. Controlling the pathways by which O_2 is activated by photogenerated electrons or holes directly determines the types of ROS generated, thereby influencing reaction selectivity [120–122].

2.4.1 Superoxide radicals

Superoxide free radicals ($\cdot O_2^-$) are usually generated by the reduction of O_2 by photogenerated electrons. These radicals exhibit mild oxidation ability, and they mainly participate in radical coupling and addition reactions; for example, they are the key species for the highly selective generation of target products, such as aldehydes and ketones [123]. From a thermodynamic perspective, the reduction potential of $O_2/\cdot O_2^-$ is −0.33 V vs. NHE. Therefore, the conduction-band position of the catalyst must be sufficiently negative to generate $\cdot O_2^-$. In PCN-222 (H_2) and other singlet-exciton MOFs, the tight packing of ligands inhibited inter-system crossing, prevented the formation of $^1O_2$, and the photocatalytic oxidation coupling of amines mainly occurred via the $\cdot O_2^-$ pathway, achieving excellent selectivity (Fig. 11(a)) [93].

2.4.2 Singlet oxygen

Singlet oxygen ($^1O_2$) is generated via the energy transfer between photogenerated excitons and O_2, without electron transfer. Therefore, this reaction is not restricted by the band position of the catalyst. $^1O_2$ is a highly active electrophilic species that can directly react with electron-rich substrates and is particularly suitable for the selective oxidation of alkenes and sulfides. It was shown that the high-density AQ ligands in the Co-AQ structure form π–π stacking within the pores, facilitating exciton migration and increasing the energy-transfer efficiency, resulting in efficient $^1O_2$ generation [124]. This process is particularly active in the reaction of oxidizing thiols to sulfoxides (Fig. 11(b)).

2.4.3 Hydroxyl radicals

·OH can be generated by the oxidation of H_2O by holes or the reduction of H_2O_2 by electrons, and they are one of the most oxidizing ROS (with a standard oxidation potential of up to 2.80 V vs. NHE). However, ·OH radicals indiscriminately activate most C–H bonds, resulting in poor selectivity. The photocatalytic oxidation of toluene by Fe-UiO-66 to produce benzoic acid mainly relies on ·OH radicals [84]. Furthermore, in the photocatalytic oxidation of methane by W_{10}@Ce-bpdc, the generated ·OH radicals ultimately oxidize methane to form formic acid [124]. To improve selectivity, ·OH generation needs to be limited or confined to a specific microenvironment. Def-CuCN/NU was regulated via the Cu monometallic site to make the O_2 activation pathway more inclined to generate ·OOH rather than ·OH, thereby avoiding excessive methanol oxidation [125]. This demonstrates that precisely regulating the ROS type is critical for achieving the highly selective oxidation of C–H bonds (Fig. 11(c)).

The three ROS types discussed above often coexist in practical photocatalytic systems, and their competitive generation critically determines reaction selectivity. The tendency to generate $\cdot O_2^-$, $^1O_2$, or ·OH depends on multiple factors. First, the catalyst's band edge positions dictate thermodynamic feasibility: The conduction band must be more negative than − 0.33 V vs. NHE to reduce O_2 to $\cdot O_2^-$, while the valence band must be more positive than +2.80 V vs. NHE to oxidize H_2O to ·OH. Second, the O_2 concentration influences the competition between electron and energy transfer: A higher O_2 concentration favors electron transfer to produce $\cdot O_2^-$, whereas energy transfer to generate $^1O_2$ is less dependent on O_2 partial pressure. Third, solvent polarity and hydrogen-bonding ability affect the stabilization of $\cdot O_2^-$ and $^1O_2$, altering their steady-state concentrations. For example, polar protic solvents tend to

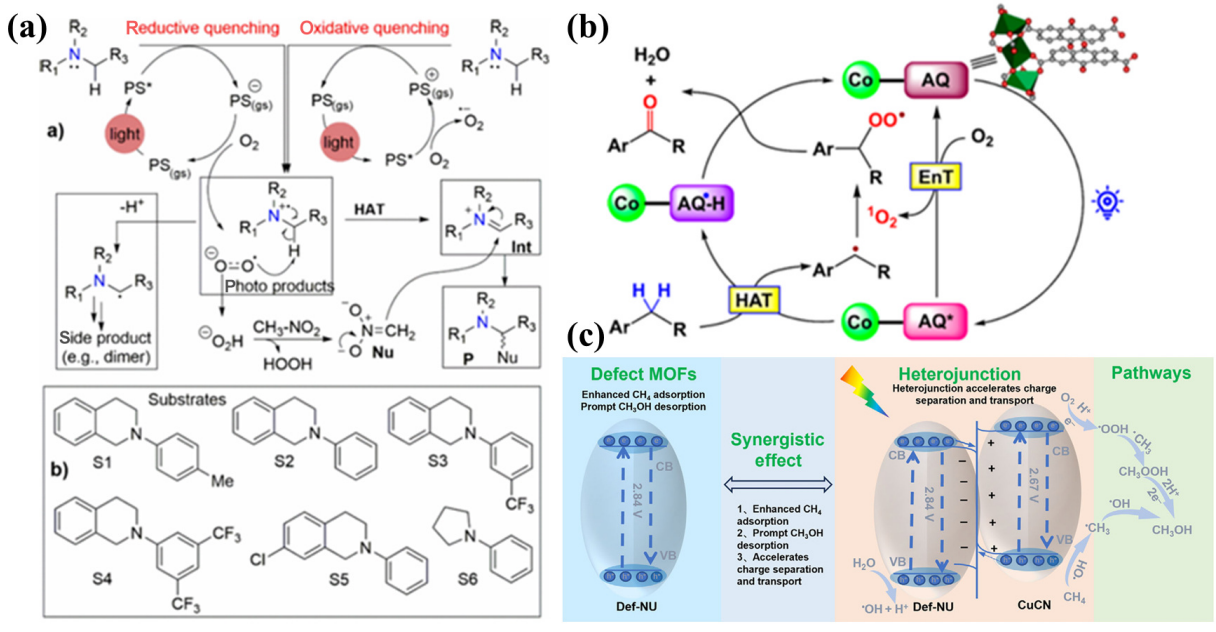

Figure 11 (a) Aza-Henry reaction through reductive or oxidative quenching of PS*, where $\cdot O_2^-$ is the dominant ROS. Adapted with permission from Ref. [93], © American Chemical Society 2025. (b) Proposed mechanism for photoactivating inert C(sp^3)–H bonds and oxygen, involving $^1O_2$ as the key species. Adapted with permission from Ref. [124], © American Chemical Society 2022. (c) Proposed reaction mechanism for CH_4 oxidation over Def-CuCN/NU, showing ·OOH as the selective ROS instead of ·OH. Adapted with permission from Ref. [103], © Feng, B. et al. 2025.

stabilize $\cdot O_2^-$ via hydrogen bonding, whereas aprotic solvents may prolong $^1O_2$ lifetimes. Finally, the MOF pore microenvironment (e.g., hydrophobicity, confined space) can selectively enrich O_2 or exclude water, thereby suppressing ·OH generation and favoring $\cdot O_2^-$ or $^1O_2$ pathways. Understanding these competitive mechanisms provides a rational basis for tuning ROS selectivity through catalyst and reaction condition design.

3 MOFs/POMOFs photocatalytic C–H bond activation reaction

This section provides an in-depth analysis of the action mechanism of MOF/POMOF catalysts based on specific reaction types and explores the structure–performance relationships of the catalysts (Table 1). Before discussing specific reaction types, it is necessary to compare the intrinsic characteristics of different C–H bonds. The bond dissociation energy of the aromatic C(sp^2)–H bond is relatively high (approximately 110–115 kcal/mol), but the conjugated system makes it prone to electrophilic substitution. Due to the hyperconjugation effect of the benzene ring, the benzyl C(sp^3)–H bond has a lower bond energy (approximately 85–90 kcal/mol) and tends to generate benzyl radicals through the HAT pathway. The allyl C(sp^3)–H bond also has a low bond energy (approximately 82–88 kcal/mol), but the presence of the double bond introduces cyclopropanation competition. Meanwhile, alkane C(sp^3)–H bonds, such as those in methane and cyclohexane (bond energies of 104 and 99 kcal/mol, respectively), are the most inert, requiring strongly oxidizing species (such as ·OH) or highly active HAT reagents (such as excited-state tetravalent tungstate). These intrinsic differences determine the selectivity requirements of different C–H bonds for ROS types ($\cdot O_2^-$, $^1O_2$, ·OH) and are also key factors in the structural design of MOF/POMOF catalysts.

3.1 Oxidation of the aromatic C(sp^2)–H bonds

The oxidation of the aromatic C(sp^2)–H bond is important for synthesizing phenols; its mechanism shares similarities with C(sp^3)–H oxidation, but the differences in electronic structure and steric hindrance bring unique challenges. Cu-based MOFs (such as

Table 1 Application of MOF/POMOF-based photocatalysts in C-H oxidation[a]

Catalyst	Reaction	Reaction conditions	Conversion (%)	Ref.
Fe-UiO-66	Toluene-benzoic acid	10 mg [P], 1 mL MeCN, 20 μL H_2O, 47.2 μmol [S], 300 W Xenon lamp (380 nm), 1 atm O_2, 25 °C, 3.5 h	96.9	[84]
Ce-AQ	Cyclohexane-cyclohexanone	5 μmol, 0.1 mmol [S], 5 mL MeCN, LED (395 nm), O_2, 25 °C, 14 h	98.4	[88]
Ce-MV^+-NS	Ethylbenzene-acetophenone	5 μmol [P],0.1 mmol [S], 5 mL MeCN, LED (455 nm), O_2, 25 °C, 14 h	83	[86]
NU-1000	THIQPh-azaHenry	10 mg [P], 0.25 mmol [S], 1 mL DMF, 0.5 mL CH_3NO_2, 15 W CFL (5 mW/cm^2), air, 2.8 h	100	[93]
Zr-NDI-H_2DPBP	Benzylamine-N-benzylidenebenzylamine	11 mg [P], 1 mmol [S], 5 mL DMF, 300 W Xenon lamp, O_2, 27 °C, 20 min	97	[95]
JNU-204	4-Cyanophenylboronic acid	1 mol% [P], 1.0 equiv [S], 2.0 epuiv Et_3N, CH_3CN/H_2O (4:1), 30 W blue LED, air, 25 °C, 48 h	93	[96]
EY@MOF-808	Benzyl alcohol-benzaldehyde	5 umol [P], 0.2 mmol [S], 3 mL MeCN, LED (455 nm), O_2, 40 °C, 12 h	68	[98]
Zn-OFDC	Benzaldehyde	0.5 mol% [P], 25 equiv [S], 0.2 mmol $C_8H_8O_2S$, 0.1 mmol C_2HCl_3O, 2 mL DMAC, blue LED (455 nm), Ar, 40 °C, 12 h	82	[99]
SD-1@PCN-Ru	Oleic acid	0.5 mg [P], 10 mmol [S], 5 mL H_2O, 2 h	93.8	[101]
CuW_{10}-TIPA	4-Methoxyphenol and p-allylanisole	10 mg [P], 0.2 mmol [S], 0.3 mmol [S], 0.24 mmol $(NH_4)_2S_2O_8$, 3 mL MeCN, white, air, 6 h	94	[106]
PW_{12}@NU-1000	CEES	1.7 μmol [P], 10 μL [S], 1 mL MeCN, 1.5 eq H_2O_2,45 °C, 20 min	98	[111]
SiW_{12}@CuMOF-1	Benzyl alcohol	0.5 mol% [P], 0.1 mmol [S], 4.5 mol% pyridine hydrochloride, 2 mL MeCN, LED (395 nm), O_2, 35 °C, 10 h	94	[112]
NENU-3a	Ethyl acetate	0.2 g [P], 30 mL 5 wt.% [S], 60 °C, 2 h	25.4	[110]
CUST-906	Cyclohexane	20 mg [P], 1 mmol [S], 9 mL MeCN, 300 W Xenon lamp, 101 kPa O_2, 72 h	33.4	[107]
NiW_{12}-TPT	Toluene	10 mg [P], 1 mmol [S], 2 mL H_2O, LED (365 nm), air, 25 °C, 24 h	99	[109]
CuW-NPY	Cyclohexane	2 μmol [P], 200 μmol [S], 1.5 mL MeCN, 500 W Xenon lamp, 101 kPa O_2, 25 °C, 12 h	86.9	[134]
PdO/TiO_2	CH_4	300 mW/cm^2	1196 μmol/(g·h)	[135]
Cu@HKUST-1	Nitrobenzene and benzaldehyde	50 mg [P], 0.2 mmol [S], 15 mg NH_3BH_3, 15 mL EtOH, 100 mW/cm^2, 10 h	100	[126]
c-Ni_5-Co_4	Nitrobenzene and benzyl alcohol	Solvent-free, visible light, 25 °C, no photosensitizer or sacrificial agent	10,552.8 μmol/g	[118]
Co-AQ	Benzyl alcohol	6 μmol [P], 0.4 mmol [S], 420 nm LED, air, 5 mL CH_3CN, 25 °C, 12 h	64	[123]
W_{10}@Ce-bpdc-2	CH_4	20 mg [P], Xenon lamp (200 mW/cm^2), O_2, 25 °C, 12 h	155 μmol/g	[124]
Def-CuCN/NU	CH_4	10 mg [P], 60 mL H_2O, Xenon lamp (200 mW/cm^2), O_2, 25 °C, 3 h	51.6 μmol	[125]
MIL-100(Fe)-200W	$N_2 + H_2O$	Visible light, H_2O, 25 °C, ambient pressure	115.1 μmol/(g·h)	[127]
PW_{12}-Cu-pbba	Indane	0.5 mol% [P], 0.1 mmol [S], 2 mL DCE, O_2, 25 °C, 48 h	81	[130]

[a][S] = substrate; [P] = photocatalyst.

HKUST-1) exhibited unique catalytic behavior in the hydroxylation of benzene to phenol [126]. The presence of water is crucial because water molecules can coordinate to the unsaturated Cu sites, activate the benzene ring through hydrogen bonds, and promote the decomposition of H_2O_2 to generate ·OH, thereby efficiently oxidizing benzene to phenol. The conversion rate of HKUST-1 without water treatment was only 2.7%, while it increased to 36.5% after water treatment, highlighting the clear influence of the coordination environment on catalytic performance (Fig. 12(a)). Fe-based MOFs (such as MIL-100(Fe)) can undergo the photoreduction of Fe^{3+} to Fe^{2+} under visible light and then generate ·OH through a Fenton-like reaction to drive the hydroxylation of benzene [127]. The conversion rate of MIL-100(Fe) reached 22.5%, and it can be reused, demonstrating the potential of MOF-based catalysts in this reaction (Fig. 12(b)).

Aromatic C(sp^2)–H hydroxylation typically requires highly oxidizing species such as ·OH, which can be generated via photo-Fenton reactions (e.g., using MIL-100(Fe)) or H_2O_2 activation at unsaturated metal sites (e.g., using HKUST-1). Unlike benzylic or aliphatic C–H bonds, the π-system of the aromatic rings makes them less susceptible to direct HAT; instead, electrophilic attack by ·OH or metal–oxo species leads to an arenium intermediate, which subsequently rearranges to phenol. To achieve high selectivity in this reaction, overoxidation to dihydroxybenzenes or quinones must be avoided, which can be partially achieved by pore confinement to limit the accessibility of the product to further oxidative attack.

3.2 Oxidation of benzyl C(sp^3)–H bonds

The C(sp^3)–H bond of the benzyl group has low bond energy (~85–90 kcal/mol) due to the superconjugation effect of the benzene ring. It is an ideal model for studying C–H activation, and its oxidation products, such as benzaldehyde and benzyl ketone, are important chemical intermediates [128]. Oxidation to ketone/alkol is the most widely studied example of such reactions. The main challenge is the selective generation of benzyl radicals and the control of their reaction pathways with ROS to avoid excessive oxidation to carboxylic acids or CO_2 [129].

Previous studies showed that in PW_{12}-Cu-pbba and Cu-P_2Mo_{18} catalysts containing Cu-POM dual-sites, t-BuOOH acts as an oxidant and is activated at the Cu site, generating t-BuO· and ·OH radicals [130, 131]. Electron paramagnetic resonance studies confirmed the existence of these radicals. The generated radicals seize hydrogen atoms from the benzene methylene position, forming benzyl radicals, and subsequently combine with O_2 or peroxides, ultimately generating benzoquinone (Fig. 13(a)). Cu-P_2Mo_{18} achieved a 90% conversion rate of benzene–methane and a 99% selectivity for benzoquinone under optimal conditions, demonstrating the efficiency of Cu-POMs cooperative catalysis. Furthermore, $^1O_2$ generated through energy transfer from Co-AQ was shown to attack the C–H bond at the benzene methylene position of benzene-methane, forming a peroxide intermediate and ultimately producing ketone [123]. This pathway avoids the generation of strongly oxidizing ·OH, resulting in extremely high selectivity (over 98%). Free-radical capture experiments confirmed that the reaction was almost completely inhibited when the $^1O_2$ capture agent DABCO was added, whereas there was no significant effect when an ·OH capture agent was added, further confirming the dominant role of $^1O_2$. A study of EY@MOF-808 showed that high selectivity was not achieved by controlling active species but rather from the differential binding ability of the MOF pore channels to substrates and products [98]. The Zr unsaturated site preferentially coordinates with the hydroxyl group of benzyl alcohol, bringing it close to the EY photosensitizer for oxidation, whereas the benzaldehyde carbonyl product only weakly coordinates with Zr and is quickly desorbed, avoiding further oxidation to benzoic acid (Fig. 13(b)). These results highlight the key role of host–guest interactions in regulating selectivity.

In summary, the selective generation of benzyl radicals and control over their reaction pathways in MOFs/POMOFs rely on three key factors. First, the choice of ROS determines the hydrogen abstraction mechanism: $\cdot O_2^-$ and $^1O_2$ tend to generate benzyl radicals with high selectivity, while ·OH often leads to overoxidation. Second, the design of active sites (e.g., Cu-POM dual

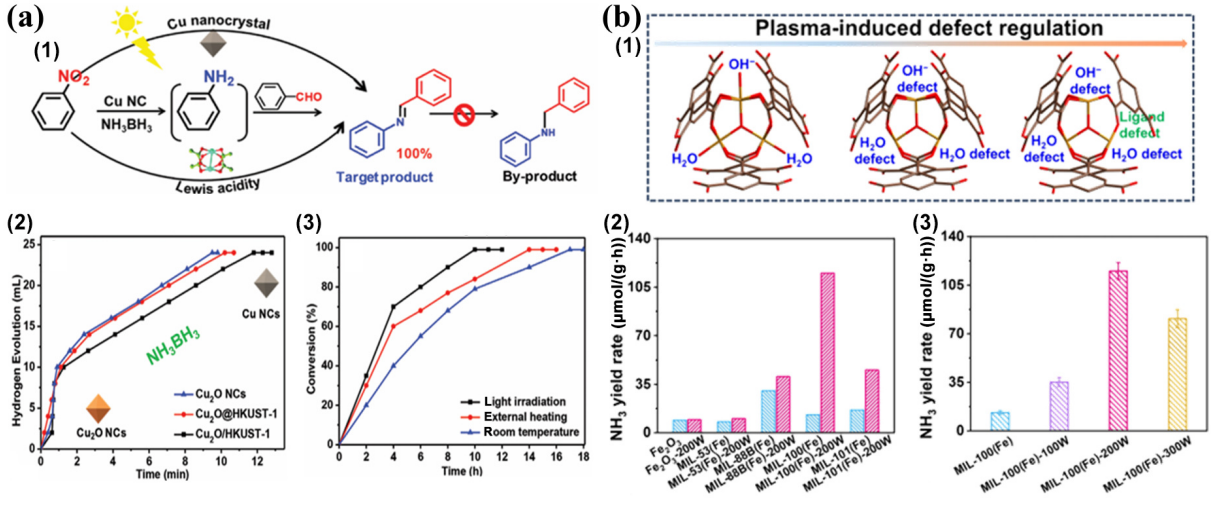

Figure 12 (a) (1) Synthesis of aromatic imines through hydrogenation of nitrobenzene and reductive amination of benzaldehyde. (2) Plots of time versus the volume of hydrogen generated from catalytic hydrolysis of NH_3BH_3 over Cu_2O@HKUST-1, Cu_2O/HKUST-1 and Cu_2O NCs. (3) Conversion of the cascade reactions under different experimental conditions. Reaction conditions: 0.2 mmol nitrobenzene, 0.2 mmol benzal dehyde, 15 mg NH_3BH_3, 50 mg catalyst, 15 mL ethanol, visible-light irradiation (100 mW/cm²). Adapted with permission from Ref. [126], © Wiley-VCH GmbH 2021. (b) (1) Schematic illustration of the plasma-assisted synthesis of MOF catalysts with different types of defects. (2) Photocatalytic NH_3 yield rates over four samples. (3) Photocatalytic NH_3 yield rates over MIL-100(Fe) and plasma-modified MIL-100(Fe) samples with different powers. Adapted with permission from Ref. [127], © Wiley-VCH GmbH 2024.

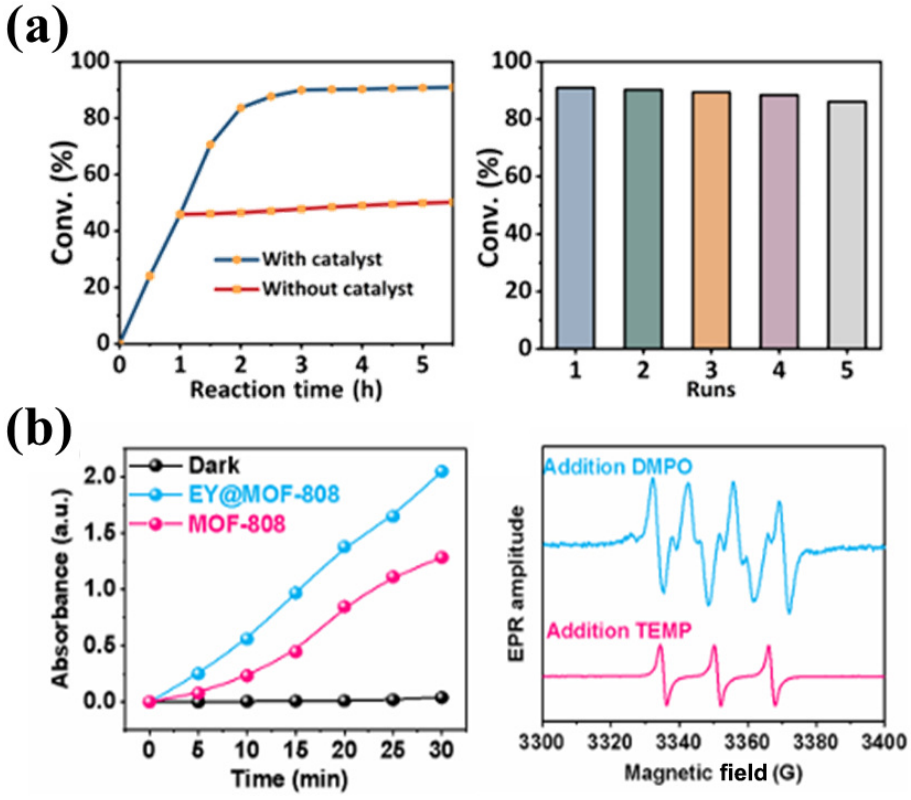

Figure 13 (a) Thermal filtration experiments and recyclability of Cu-P_2Mo_{18} for the diphenylmethane oxidation reaction. Adapted with permission from Ref. [131], © American Chemical Society 2025. (b) Time-dependent corresponding absorption of 3,3′,5,5′- tetramethylbenzidine (TMB) at 393 nm in a CH_3CN solution containing MOF-808 and EY@MOF-808 with 455 nm irradiation and EY@MOF-808 without light irradiation in the air atmosphere. Electron paramagnetic resonance (EPR) spectra of EY@MOF-808 for the $^1O_2$ and $\cdot O_2^-$ detection in the presence of 2,2,6,6-tetramethylpiperidine (TEMP) and 5,5-dimethyl-1-pyrroline-N-oxide (DMPO). Adapted with permission from Ref. [98], © American Chemical Society 2024.

sites and Co-AQ for energy transfer) controls the activation pathway of the oxidant (t-BuOOH or O_2) and the subsequent fate of the radical. Third, pore confinement and host–guest interactions regulate substrate binding and product desorption, as demonstrated by EY@MOF-808, for which the preferential coordination of benzyl alcohol over benzaldehyde suppresses further oxidation. These principles provide a rational basis for designing catalysts with high selectivity toward ketones or aldehydes in benzylic C–H oxidation.

3.3 Oxidation of the allyl C(sp^3)–H bonds

The C(sp^3)–H bond at the allyl position has a lower bond energy (approximately 82–88 kcal/mol) than that at the benzyl position due to the conjugation of the double bond. Its oxidation product is an important intermediate for the synthesis of fragrances and pesticides. Cyclohexene is often used as a model substrate, and its oxidation faces competition between the epoxidation of the olefin double bond and the oxidation at the allyl position [132]. Ce-AQ exhibited high selectivity for the oxidation of allylic positions when oxidizing cyclohexene, with 2-cyclohexene-1-ketone formed as the main product [88]. Mechanistic studies indicated that photogenerated holes or generated ·OH tended to seize the hydrogen at the allylic position rather than directly reacting with the double bond. DFT calculations further revealed that the energy barrier for hydrogen extraction from the allylic C–H bond is lower than that of cyclohexene ring oxidation, which was highly consistent with the experimental results (Fig. 14).

In allylic C–H oxidation, the presence of a C=C double bond introduces competition between epoxidation and allylic hydrogen abstraction. To achieve high selectivity for allylic oxidation, HAT must be favored over electrophilic addition to the double bond. This can be accomplished using ROS with suitable hydrogen-abstraction ability but low electrophilicity, such as $\cdot O_2^-$ or photogenerated holes, or by employing HAT-active species (e.g., W–O· from decatungstate). Additionally, the confinement effect of MOF pores can sterically shield the double bond while exposing allylic C–H bonds, as proposed for Ce-AQ [88]. The lower bond dissociation energy of allylic C–H bonds (~ 82–88 kcal/mol) than vinyl C–H bonds further favors HAT, but careful catalyst design is required to suppress unwanted epoxidation pathways.

3.4 Oxidation of C(sp^3)–H bonds in alkanes

The oxidation of alkanes (such as methane and cyclohexane) is the most challenging goal in this field. The C–H bonds in alkanes are extremely inert (with a bond energy up to 104 kcal/mol in methane), which imposes strict catalyst-design requirements [133].

3.4.1 Cyclohexane oxidation

The oxidation of cyclohexane to cyclohexanol and cyclohexanone (ketone-alcohol (KA) oil) is an important process in the industrial production of nylon-66. The traditional process has a conversion rate of only ~ 4% and a selectivity of ~ 70%. Ten-poly tungstate-based MOFs exhibit excellent performance in this reaction. The proposed photocatalytic mechanism of catalysts such as CUST-906 and CuW-NPY involves the excitation of $[W_{10}O_{32}]^{4-}$ under light irradiation to generate W–O intermediates, which seize the hydrogen atoms of cyclohexane via HAT to generate cyclohexyl

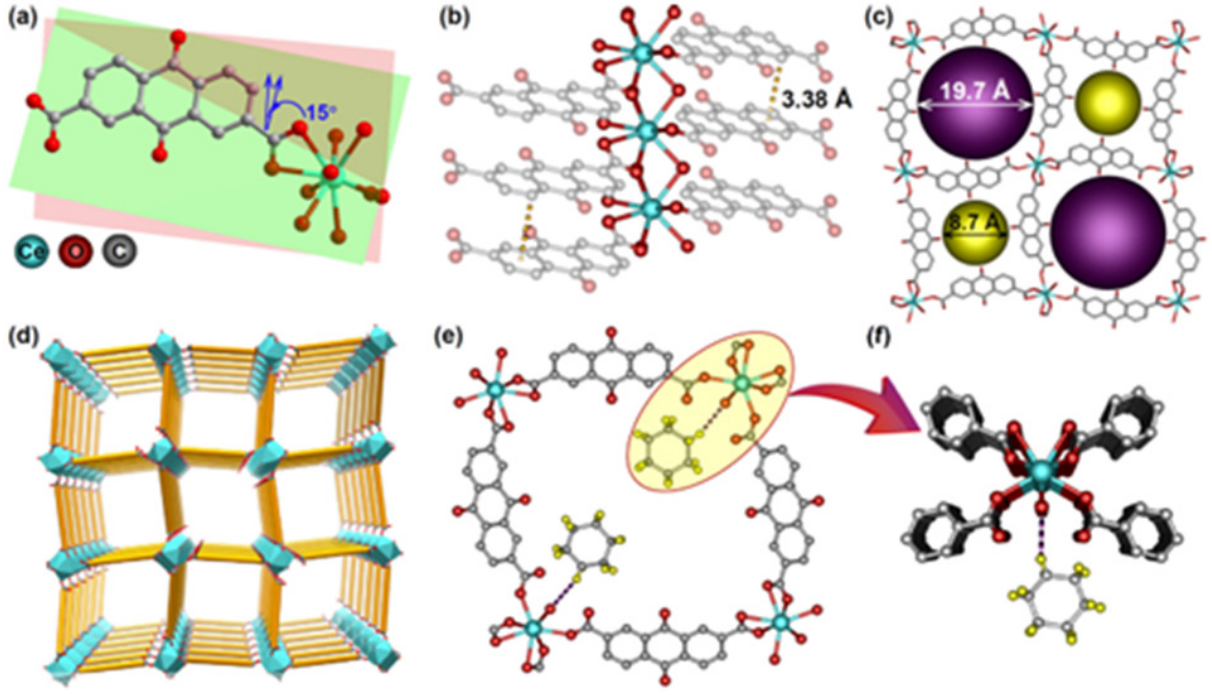

Figure 14 (a) Coordination model between the anthraquinone ligand and cerium ion in Ce-AQ. (b) Oxygen bridge groups of Ce-O-Ce in Ce-AQ and the parallel-displaced π–π interaction between the adjacent anthraquinone groups with a distance of 3.38 Å. (c) Two different size windows in the MOF. (d) Pores of the 3D framework in Ce-AQ along the *c* direction. (e) Cyclohexane-encapsulated co-crystal structure of CYH@Ce-AQ. (f) Interaction between the cyclohexane and binuclear cerium oxygen bridge of Ce-AQ. Adapted with permission from Ref. [88], © American Chemical Society 2022.

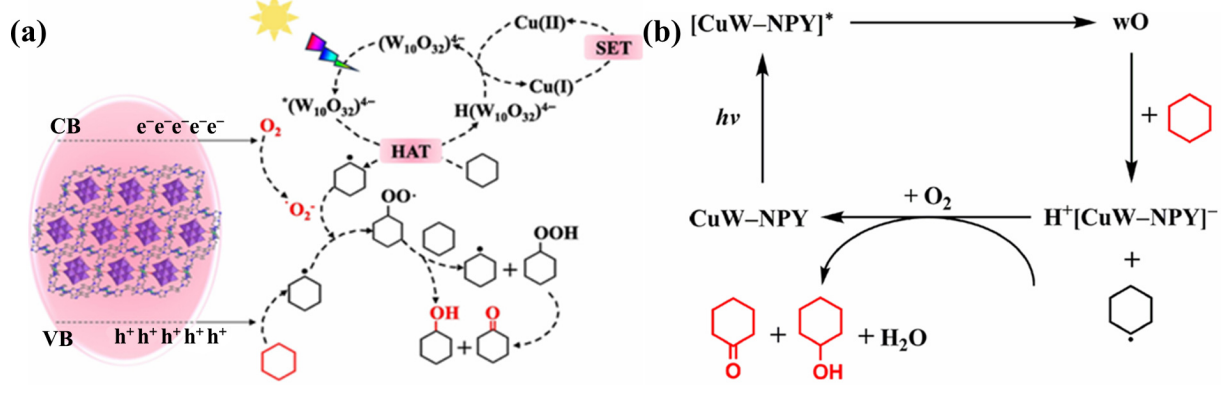

Figure 15 (a) Photocatalytic mechanism of oxidation of cyclohexane to KA oil. Adapted with permission from Ref. [107], © Elsevier Inc. 2025. (b) Proposed reaction mechanism of CuW-NPY for the photo-oxidation of cyclohexane. Adapted with permission from Ref. [134], © Springer Science+Business Media, LLC, part of Springer Nature 2020.

radicals, which then combine with O_2 to form KA oil (Fig. 15(b)) [134]. Under optimized conditions, CUST-906 achieved a cyclohexane conversion rate of 33.4% and KA oil selectivity of over 99% through the generation of $\cdot O_2^-$ free radicals, which exceeds the selectivities achieved by industrial processes [107]. Spectroscopic studies indicated that the lifetime of the W–O intermediate was approximately several tens of nanoseconds, which is sufficiently long to enable collisions with the substrate (Fig. 15(a)).

3.4.2 *Methane oxidation*

MOFs/POMOFs exhibit great potential in methane oxidation. The Def-CuCN/NU catalyst was designed to integrate engineered defects, single atomic sites, and S-type heterojunctions, successfully resolving the trade-off between high activity and high selectivity in methane oxidation [125]. The key to its success is the use of defective MOFs as microreactors, where the mesoporous structure enhances the adsorption of CH_4 and promotes the rapid desorption of CH_3OH, effectively inhibiting overoxidation (Fig. 16(a)).

Comparing methane and cyclohexane oxidation highlights distinct catalyst-design requirements. Methane has a higher C–H bond energy (104 vs. 99 kcal/mol for cyclohexane) and a much smaller molecular size, making it more difficult to activate and prone to overoxidation due to the high reactivity of the initial products (methanol, formic acid, CO_2). Therefore, methane oxidation demands catalysts with strong oxidizing capacity (e.g., ·OH or high-energy HAT species) to break the strong C–H bonds. The precise control over the O_2 activation pathway avoids ·OH overproduction. An optimal adsorption–desorption balance facilitates methanol desorption before further oxidation. In contrast, cyclohexane is more easily activated via HAT, and the desired

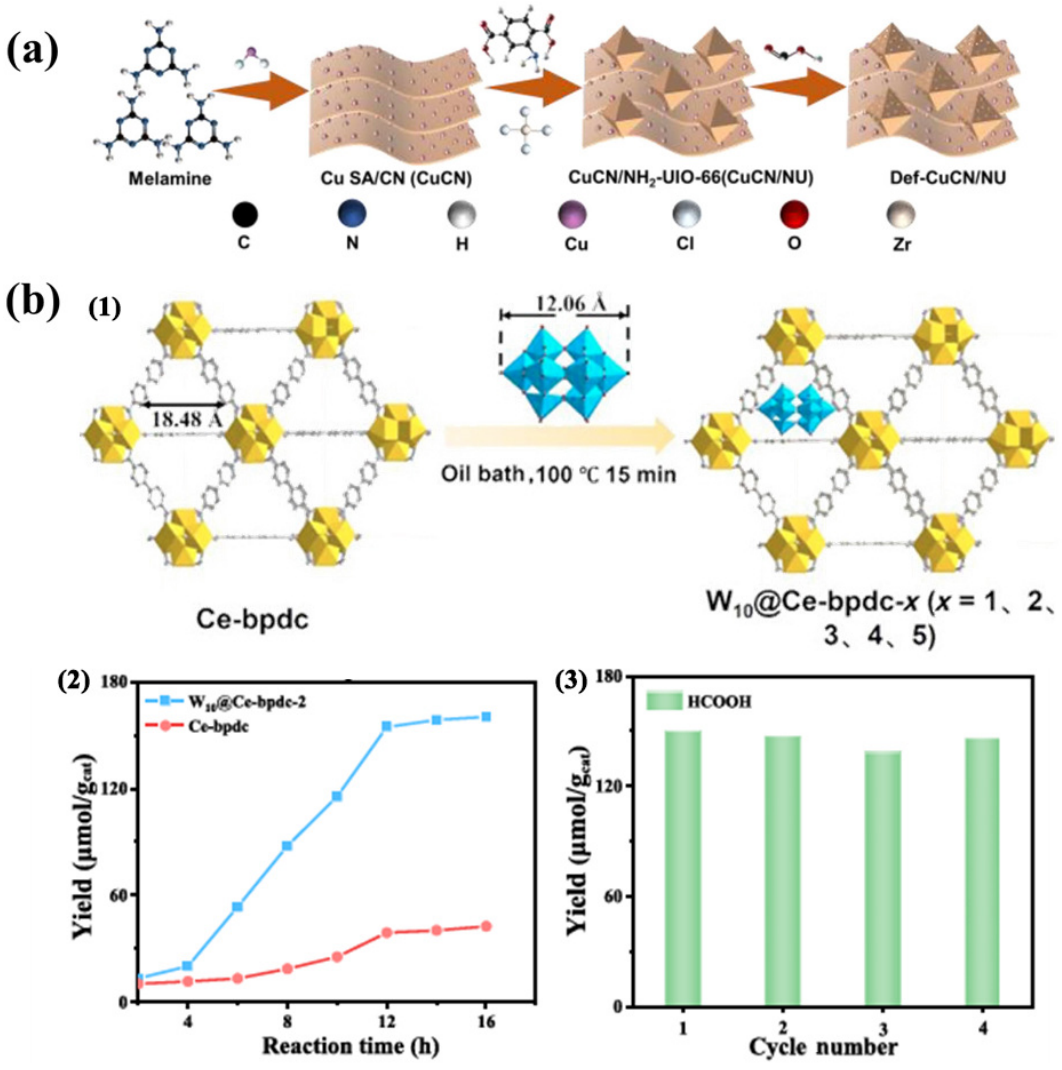

Figure 16 (a) Schematic diagram of synthesis of Def-CuCN/NU. Adapted with permission from Ref. [125], © Feng, B. et al. 2025. (b) (1) Schematic for the fabrication of W_{10}@Ce-bpdc. (2) Time-dependent HCOOH yield over W_{10}@Ce-bpdc-2 and Ce-bpdc. (3) Recycle experiments for CH_4 photooxidation. Adapted with permission from Ref. [124], © Published by Elsevier B.V. on behalf of Chinese Chemical Society and Institute of Materia Medica, Chinese Academy of Medical Sciences 2025.

products (cyclohexanol/cyclohexanone) are relatively stable; thus, the main challenge lies in achieving high selectivity toward KA oil while suppressing ring-opening reactions or overoxidation. Accordingly, POMOFs, such as CUST-906 and CuW-NPY, effectively utilize decatungstate-mediated HAT for cyclohexane production, whereas methane oxidation requires more sophisticated designs, such as the combination of engineered defects, single-atom sites, and heterojunctions in Def-CuCN/NU to regulate ROS generation and product desorption [125].

Formic acid was synthesized by methane oxidation using the W_{10}@Ce-bpdc catalyst at room temperature with O_2 as the oxidant, resulting in a formic acid yield of 155 μmol/g [135]. Mechanistic studies indicated that Ce-MOF absorbs light energy to generate separated charges; the electrons are captured by W_{10} through the Ce(III)/Ce(IV) cycle, which then reduces O_2 to generate H_2O_2. This work revealed a new pathway for methane oxidation and provided new strategies for methane conversion under mild conditions (Fig. 16(b)) [124]. Furthermore, the use of a PdO/TiO_2 nanocomposite was demonstrated as a new pathway for the nonoxidative coupling of methane [135]. The photogenerated holes on TiO_2 generate O^- active sites, which seize the H in CH_4 to generate $\cdot CH_3$, which is stabilized on the PdO surface and undergoes C–C coupling to form C_2H_6. DFT calculations indicated that the adsorption energy of PdO for $\cdot CH_3$ is moderate, which may stabilize the free radicals to prevent excessive oxidation and promote the coupling reaction (Fig. 17).

3.5 Series connection of photocatalytic oxidation and other transformations

By taking advantage of the simultaneous generation of electrons and holes during photocatalysis, the efficient coupling of oxidation and reduction half-reactions can be achieved, thereby converting solar energy into chemical energy while maximizing the atomic economy [136].

3.5.1 Oxidation–reduction series

The c-Ni_5-Co_4 catalyst was used to couple the reduction of nitrobenzene with the oxidation of benzyl alcohol, resulting in the formation of aniline and benzaldehyde (Fig. 18(a)) [118]. These compounds then underwent further condensation to form imines. This design fully utilizes the photogenerated electrons and holes for

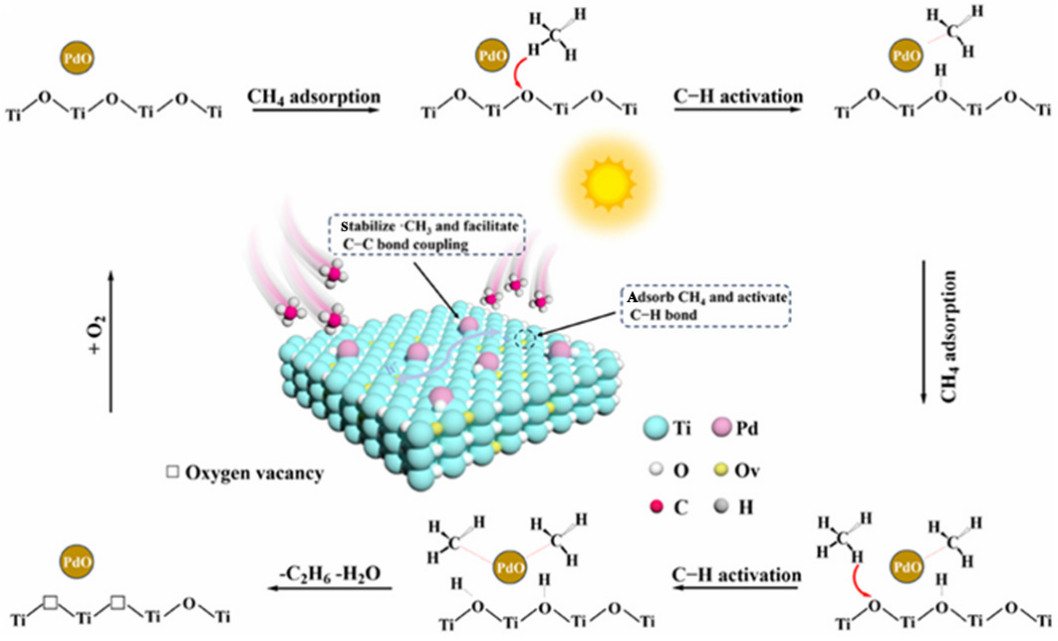

Figure 17 Proposed photocatalytic mechanism of the NOCM reaction over PdO/TiO_2. Adapted with permission from Ref. [135], © The Royal Society of Chemistry 2026.

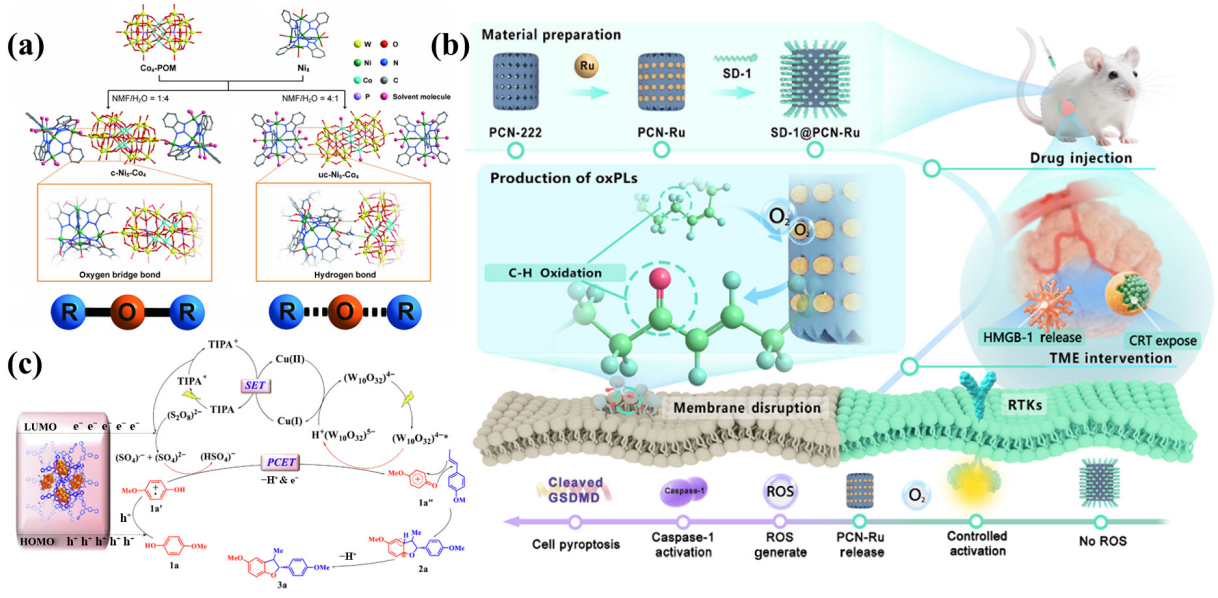

Figure 18 (a) Crystal structures of Co_4-POM, Ni_5, c-Ni_5-Co_4, and uc-Ni_5-Co_4. Adapted with permission from Ref. [118], © Science China Press 2024. (b) Proposed photocatalytic mechanism of photocatalytic the oxidative [3+2] cycloaddition of phenols with olefins. Adapted with permission from Ref. [106], © Elsevier Inc. 2024. (c) The intelligent host-guest system (SD-1@PCN-Ru) for targeted RTKs recognition and controlled membrane phospholipid oxidation. Adapted with permission from Ref. [101], © Wiley-VCH GmbH 2026.

the reduction of 6-electron nitrobenzene and the oxidation of 2-electron benzyl alcohol, respectively. The two hybrids undergo condensation to form the final product. Isotope labeling experiments confirmed that the nitrogen and carbon in the product come from nitrobenzene and benzyl alcohol, respectively. The c-Ni_5-Co_4 catalyst achieved an imine yield of 10,552.8 μmol/g under anhydrous conditions, which is 500 times that obtained for a physical mixture.

3.5.2 *Ring-addition reactions*

CuW_{10}-TIPA was used to catalyze the [3+2] cycloaddition of phenol and alkenes, providing a green synthetic route for constructing a biologically active dihydrobenzofuran skeleton (Fig. 18(c)) [106]. Mechanistic studies indicated that this reaction involves the oxidation of phenol by photogenerated holes to form phenol oxygen radicals, which then undergo cycloaddition with activated alkenes, rather than following the traditional HAT process. Free-radical trapping experiments confirmed the formation of phenol oxygen radicals. The catalyst showed good adaptability to various substituted phenols and alkenes, with a yield of 94%, and was recycled 5 times without significant deactivation.

3.5.3 *Cancer treatment*

A remarkable extension of photocatalytic oxidation into the field of biomedicine was demonstrated using the SD-1@PCN-Ru catalyst [101]. Guided by the targeted probe SD-1, the photocatalyst precisely located the overexpressed Receptor Tyrosine Kinase (RTK) receptors on cancer-cell membranes and generated ROS under light excitation, selectively oxidizing membrane phospholipids. Lipidomic analysis indicated that the concentrations of the two main types of membrane phospholipids, phosphatidylcholine (PC) and phosphatidylethanolamine (PE), significantly decreased, and the membrane integrity was disrupted, ultimately resulting in cell pyroptosis and immune-response activation. This cross-disciplinary application demonstrates the great potential of MOF host–guest chemistry in the field of biomedicine and proves that photocatalytic oxidation can be extended from organic synthesis to life science, providing new tools for precise treatments (Fig. 18(b)). Although this system operates in a biological context, the core chemical process is ROS-mediated C–H bond oxidation: The photogenerated species ($\cdot O_2^-$ or $^1O_2$) abstract hydrogen atoms from the allylic C–H bonds of unsaturated phospholipids, converting them into C–O bonds and disrupting membrane integrity. This demonstrates that the principles of photocatalytic C–H activation can be extended beyond traditional organic synthesis to biomedical applications.

3.6 Catalyst stability and recyclability

The cyclic stability of catalysts is a key parameter for evaluating their viability for practical application. The representative catalysts reviewed in this article exhibit excellent recyclability. For instance, PW_{12}-Cu-pbba shows no significant decrease in activity after 5 cycles of benzyl C–H oxidation (Fig. 13(a)) [130]. Cu-P_2Mo_{18} was recycled 5 times for benzene methanation, and powder XRD and Fourier-transform infrared spectroscopy analyses indicated that the structure remained intact [131]. EY@MOF-808 was reused 5 times for benzyl alcohol oxidation, and the conversion rate and selectivity remain unchanged [98]. In the [3+2] cycloaddition reaction of phenol with alkenes catalyzed by CuW_{10}-TIPA, the yield remained over 90% after 5 cycles [106]. In a methane oxidation system, W_{10}@Ce-bpdc maintained 85% of the initial acetic-acid yield after 4 cycles (Fig. 16(b)) [124]. Furthermore, MIL-100(Fe) exhibited stable activity during various benzyl hydroxylation cycles [127]. These results indicate that MOF/POMOF materials can effectively maintain stable catalytic active sites owing to their structural rigidity and effective encapsulation.

4 Conclusion and outlook

4.1 Conclusion

Over the past decade, MOFs and POMOFs have achieved various milestones in photocatalytic C–H bond activation. The core insights are summarized as follows (Fig. 19).

First, in addition to the composition, the structure determines the catalyst function. Catalytic performance relies on both the type of elements as well as their precise arrangement, electronic coupling, and pore microenvironment. Even a single missing atom (defect), ligand orientation, or POM encapsulation position can fundamentally alter catalytic behavior.

Second, charge regulation is fundamental in photocatalysis. Every step, including light absorption, charge separation, and surface reactions, requires precise control over photogenerated electrons and holes. Strategies such as the use of D–A ligands, POMs as electron sponges, and heterojunctions aim to promote effective charge separation and steer carriers to specific active sites.

Third, selectivity is achieved by the precise control of reaction pathways. High selectivity requires the careful selection of ROS ($\cdot O_2^-$ vs. $\cdot$OH vs. $^1O_2$), specific substrate recognition, and rapid product desorption. The pore-confinement effect of MOFs/POMOFs provides unprecedented scope for such regulation.

Fourth, synergistic effects are critical to overcome performance bottlenecks. For example, dual-metal-sites, POM–MOF structures, and host–guest systems all provide synergistic effects. The coupling of oxidation with reduction half-reactions further demonstrates that future catalyst designs should emphasize multicomponent integration and multifunctional coupling.

In summary, MOFs and POMOFs offer a structurally tunable platform that addresses the long-standing activity–selectivity trade-off faced by C–H bond activation. Continued advances in precise synthesis, operando characterization, and data-driven design are expected to unlock their potential for sustainable chemical synthesis.

4.2 Outlook

Despite remarkable achievements, this field faces several challenges that urgently need to be overcome.

(1) Operando characterization techniques. The development of novel POMOFs is critical in this field. As for MOFs/POMOFs, the mechanisms are often inferred by characterizing the catalyst and comparing the reagents before the reaction with the products after the reaction. However, practical catalytic processes are dynamic and transient. In the future, the use of advanced spectroscopic techniques under working conditions, such as operando X-ray absorption spectroscopy, ultrafast two-dimensional (2D) infrared spectroscopy, and transient absorption spectroscopy, should be combined with high-precision theoretical calculations to capture the electronic state and geometric structure changes of the active center during the reaction process in real time, especially the evolution of transient intermediates, to unveil the fundamental catalytic cycle.

(2) Precision synthesis. Current selectivity strategies focus on distinguishing C–H bonds in different chemical environments (such as benzyl vs. alkyl). Future research could draw on our knowledge of biological enzymes to design more complex pore environments. Revolutionary strategies for the synthesis of chiral drugs and fine chemicals could be achieved by introducing chiral pockets, hydrogen bond networks, and hydrophobic microregions to achieve stereoselective and regioselective recognition and the activation of C–H bonds at different positions and spatial orientations within the same molecule.

(3) Green and scalable synthesis. The synthesis of most MOF/POMOF catalysts remains at the laboratory scale and uses expensive ligands, solvents, and metal sources. Developing green, low-cost, and scalable synthesis methods, such as aqueous-phase, mechanochemical, and continuous-flow synthesis, and evaluating the long-term stability, space-time yield, and environmental effects of catalysts in continuous-flow reactors are necessary to promote industrial applications. The successful application of NiW_{12}-TPT in kilogram-scale reactions and the room-temperature aqueous-phase synthesis of UiO-66-type MOFs highlight positive advancements.

(4) Diversification beyond C–H oxidation. This review focuses

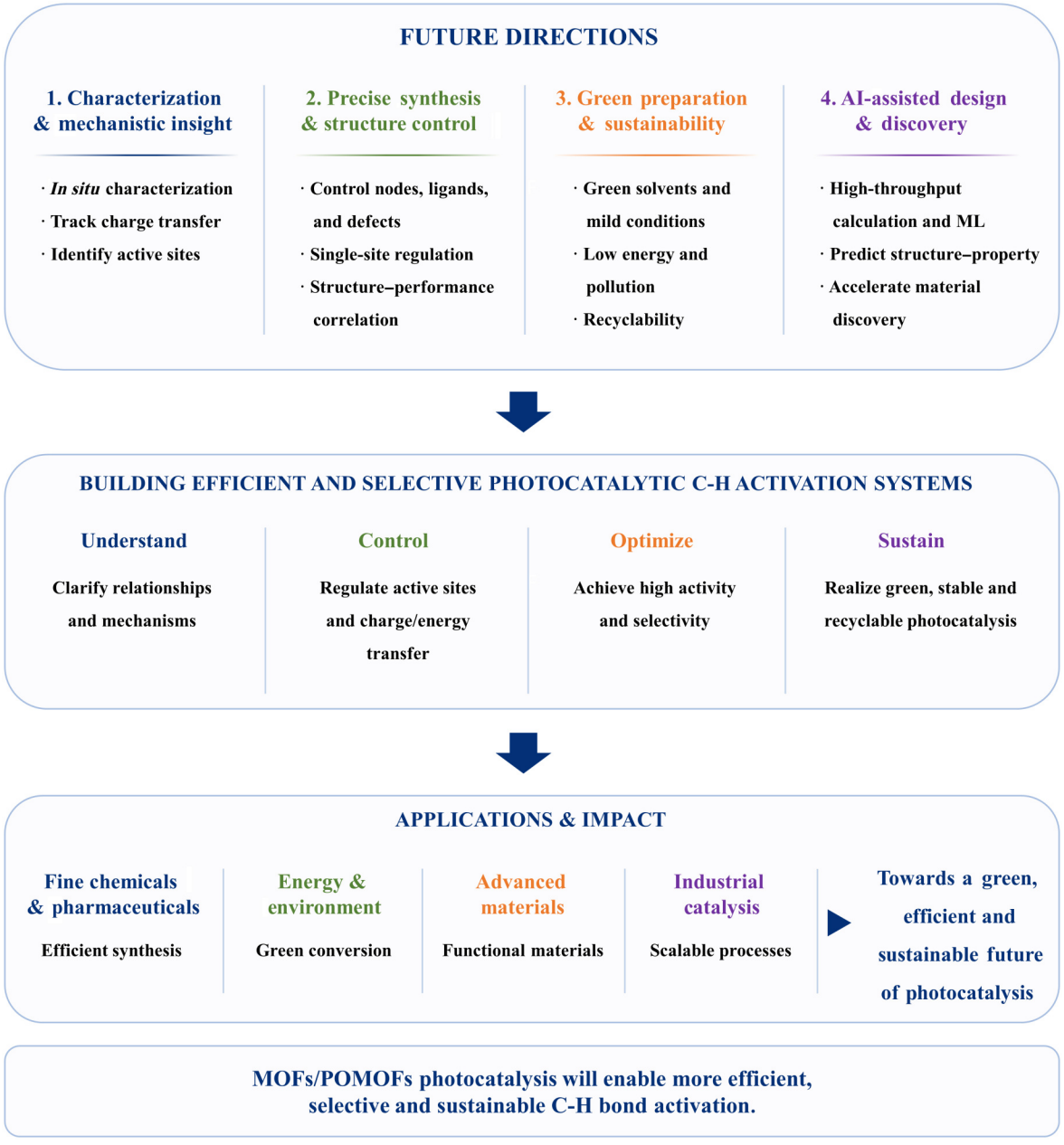

Figure 19 Outlook for light-mediated C-H bond activation with MOFs/POMOFs.

on the generation of C–O bonds, but the potential of photogenerated radical intermediates R· extends far beyond this. The utilization of R· to construct bonds, such as C–C, C–N, and C–X, and achieve the direct functionalization diversity of C–H bonds, will be an exciting future direction. In the future, the photocatalytic functionalization of C–H bonds is expected to be combined with other reaction types to produce diverse molecular structures.

(5) Artificial-intelligence (AI)-assisted material design. With the accumulation of MOF/POMOF structure databases and catalytic performance datasets, machine learning and AI are expected to advance catalyst design. By establishing structure–performance relationship models, conducting high-throughput screening of potential high-performance catalysts, and combining with experimental verification, the discovery of new materials will be greatly accelerated.

Looking to the future, the design of MOF/POMOF photocatalysts is expected to become more intelligent, precise, and functional. We confidently predict that through the continuous innovation of these molecular materials and the use of unlimited sunlight, highly stable C–H bonds could be transformed into highly complex molecular structures. These advancements will significantly contribute to the development of a sustainable chemical industry and green synthesis paradigm.

Data availability

Not applicable.

Acknowledgements

This work was financially supported by the National Natural Science Foundation of China (No. 22271023) and Jilin Province

Science and Technology Development Plan Project-Construction of innovation capacity (No. YDZJ202502CXJD051).

Declaration of competing interest

The authors declare that they have no known competing financial interests or personal relationships that could have appeared to influence the work reported in this paper. Author Zhongmin Su is the advisory board member of this journal, but he is not involved in the peer-review or decision of this article.

Author contribution statement

Y. J. L.: Writing – original draft, supervision, investigation. X. Y. Z.: Validation, investigation. J. S.: Supervision, funding acquisition, writing – review & editing. W. X. Z.: Investigation. X. L.: Methodology, Writing – review & editing. Z. M. S.: Funding acquisition, writing – review & editing.

Use of AI statement

None.

References

[1] Rogge, T.; Kaplaneris, N.; Chatani, N.; Kim, J.; Chang, S.; Punji, B.; Schafer, L. L.; Musaev, D. G.; Wencel-Delord, J.; Roberts, C. A. et al. C–H activation. *Nat. Rev. Methods Primers* **2021**, *1*, 43.

[2] Qi, Z.; Wu, X. F.; Li, Q.; Lu, C. S.; Carabineiro, S. A. C.; Zhao, Z. W.; Liu, Y.; Lv, K. L. Singlet oxygen in environmental catalysis: Mechanisms, applications and future directions. *Coord. Chem. Rev.* **2025**, *529*, 216439.

[3] Qin, Y.; Zhu, L. H.; Luo, S. Z. Organocatalysis in inert C–H bond functionalization. *Chem. Rev.* **2017**, *117*, 9433–9520.

[4] Meng, S. Q.; Li, Z. Y.; Du, Y. C.; Cheng, X.; Nian, B. B.; Fu, S. Y.; Song, X. F.; Cui, H. Y. Empowering precision C–H functionalization: Advances in peroxygenase engineering. *Angew. Chem., Int. Ed.*, in press, DOI: 10.1002/anie.202525086.

[5] Shang, Q. Q.; Shen, K. Q.; Zhao, D. Y.; Wang, X. Y.; Wei, Y. T.; Wang, H. Y.; Wang, G.; Zhang, D. D.; Niu, J. Y. Rare-earth-induced peroxo-phosphotungstates: Enhanced proton conductivity in corresponding membranes. *Polyoxometalates* **2025**, *4*, 9140077.

[6] Kang, S. Y.; Lv, X. L.; Shi, Z. Z. Cyclopropane-to-organoboron conversion via C–H and C–C bond activation. *Chem. Soc. Rev.* **2026**, *55*, 1915–1934.

[7] Shang, R.; Ilies, L.; Nakamura, E. Iron-catalyzed C–H bond activation. *Chem. Rev.* **2017**, *117*, 9086–9139.

[8] Kalita, R.; Thadhani, C.; Manna, K. Architecting metal-organic framework-based/derived catalysts for methane functionalization. *ACS Catal.* **2026**, *16*, 882–909.

[9] Eisenstein, O.; Milani, J.; Perutz, R. N. Selectivity of C–H activation and competition between C–H and C–F bond activation at fluorocarbons. *Chem. Rev.* **2017**, *117*, 8710–8753.

[10] Yan, Z. L.; Ma, C. Y.; Chen, S. H.; Chen, C.; Li, S. Y.; Meng, W. W.; Hou, Z. H.; Song, M. Y.; Jiang, G. B. Synergy between Brønsted acid sites and Cu/Zn single-atom sites in zeolite for the direct oxidation of methane. *J. Am. Chem. Soc.* **2026**, *148*, 17753–17763.

[11] Yang, Y. D.; Lan, J. B.; You, J. S. Oxidative C–H/C–H coupling reactions between two (hetero)arenes. *Chem. Rev.* **2017**, *117*, 8787–8863.

[12] Li, T. B.; Zhang, Q.; Zhong, Y. F.; Min, X. T.; Guo, Y. L.; Qin, M. Y.; Wang, H.; Li, S. X.; Cui, Y. T.; Lu, S. J. et al. Selective aerobic oxidation of C–H bond over C–C bond on Pd_1/Mn_2O_3 single-atom catalysts. *ACS Catal.* **2026**, *16*, 7454–7464.

[13] Huang, H.; Wang, C. C.; Shen, W. M.; Xie, D. F.; Gong, Z.; Yi, H.; Wu, P.; Guo, M. Li^+ promoted the cyanation of unactivated C–H bonds catalyzed by the manganese porphyrin complex through biomimetic oxidation. *J. Am. Chem. Soc.* **2026**, *148*, 11893–11904.

[14] Li, S. C.; Hou, J. X.; Cao, C. S.; Wen, W.; Zhang, L.; Yang, F. F.; Chen, J. B.; Yao, J. N.; Xie, Z. L. Orbital engineering in single-atom catalysts for benzene to phenol oxidation. *ACS Catal.* **2026**, *16*, 6477–6488.

[15] Wu, W. T.; Zhang, H. N.; Wang, S.; Li, Y.; Qin, H. J.; Wang, M. W.; Chen, Q. H.; Zheng, B. S.; Zhu, S. X.; Zhang, P. Y. et al. FeCu dual-single-atom catalyst promotes gradient H_2O_2 activation for enhanced methane oxidation to methanol. *Nat. Commun.* **2026**, *17*, 3526.

[16] Zang, D. J.; Wang, H. Q. Polyoxometalate-based nanostructures for electrocatalytic and photocatalytic CO_2 reduction. *Polyoxometalates* **2022**, *1*, 9140006.

[17] Biswas, S.; Isakov, A.; Dias, N.; Finn, M. T.; Cokas, J.; Epshteyn, A.; Alexandrova, A. N.; Ahmed, M.; Kaiser, R. I. Low-temperature non-oxidative coupling of methane on atomically dispersed titanium-aluminum-boron nanopowder. *J. Am. Chem. Soc.* **2026**, *148*, 10205–10215.

[18] He, J. B.; Wu, L.; Yuan, W. L.; Pan, H. X.; Wang, B. J.; Tang, G. L. Molecular basis of regioselective bridgehead C(sp^3)-H bond hydroxylation by P450 peroxygenase in bicyclomycin biosynthesis. *ACS Catal.* **2026**, *16*, 5616–5629.

[19] Ye, P.; Xiong, L. N.; Cui, Y. Q.; Mao, Y. J.; Zhang, Y. L.; Xu, Z. Y.; Luo, Y.; Xu, D. Q.; Lou, S. J. Enantioselective C–H arylation for axially chiral tetra-*ortho*-substituted heterobiaryl *N*-oxides. *J. Am. Chem. Soc.* **2026**, *148*, 11609–11620.

[20] Li, H. S.; Bai, J. Y.; Wang, F.; Li, X. X.; Wang, M. Y.; Li, X. W. Harnessing cooperative hydrogen-atom transfer and nitrene-primed radical-polar crossover for asymmetric C–H amidation of α-amino carbonyls. *J. Am. Chem. Soc.* **2026**, *148*, 7905–7918.

[21] Li, M. J.; Cheng, Z. W.; Wang, F. T.; Ye, J. Y.; Cheng, J.; Zhou, Z. Y.; Sun, S. G.; Wang, T. Spectator anion accelerates electrocatalytic C–H dissociation by modulating the local hydrogen bonding interaction. *ACS Catal.* **2026**, *16*, 3618–3627.

[22] Yin, Y. A.; Chen, W. J.; Liu, C. Y.; Zhang, M. M.; Lin, C. G.; Miras, H. N.; Song, Y. F. Supramolecular assembly of covalently modified Anderson-type polyoxometalates and crown ethers towards *pseudo*-rotaxane structures. *Polyoxometalates* **2025**, *4*, 9140081.

[23] Decandia, G.; Albano, G.; Gugujonović, K.; Leeb, E.; Punzi, A.; Cotugno, P.; Pò, R.; Biagini, P.; Gaeta, C.; Irimia-Vladu, M. et al. A fast and convenient synthesis of heterocycle-based polymers via infrared irradiation-assisted direct C–H bond arylation polymerization in quasi-solvent-free conditions. *J. Am. Chem. Soc.* **2026**, *148*, 5953–5965.

[24] Qiu, W. H.; Liu, C.; Zhu, J. D.; Li, W. Y.; Zou, S. H.; Li, C.; Huang, Y. Y.; Yang, K.; Song, Q. L. Iridium-catalyzed B–H/C–H dehydrogenative coupling to enable boron-nitrogen-embedded polycyclic aromatic hydrocarbons. *J. Am. Chem. Soc.* **2026**, *148*, 3015–3025.

[25] Holmberg-Douglas, N.; Nicewicz, D. A. Photoredox-catalyzed C–H functionalization reactions. *Chem. Rev.* **2022**, *122*, 1925–2016.

[26] Bellotti, P.; Huang, H. M.; Faber, T.; Glorius, F. Photocatalytic late-stage C–H functionalization. *Chem. Rev.* **2023**, *123*, 4237–4352.

[27] Cheng, Y.; Qin, K. J.; Zang, D. J. Polyoxometalates based nanocomposites for bioapplications. *Rare Met.* **2023**, *42*, 3570–3600.

[28] Lin, X. F.; Zheng, J. X.; Wang, L. W.; Wang, J.; Jiang, D.; Yamauchi, Y.; Zhang, C. Q.; Yuan, Z. H. Advances and mechanistic insights into covalent organic framework-mediated photocatalysis for organic transformations. *ACS Catal.* **2026**, *16*, 57–97.

[29] Wang, Y. X.; Zhang, Y. Y.; Liu, Y.; Wu, Z. B. Sustainable valorization of methane via photocatalysis: A review on the advances in various conversion pathways. *J. Energy Chem.* **2026**, *113*, 821–842.

[30] Li, Z. W.; Liu, B. Y.; Li, H. Y.; Xu, M. Z.; Huang, H. B. Surface polarons for synergistic kinetic and thermodynamic C–H bond oxidation. *J. Am. Chem. Soc.* **2026**, *148*, 9773–9783.

[31] Zhao, Q.; Mao, D. A.; Huang, L. L.; Zhou, K.; Tian, H. R.; Chen, B. K.; Bi, Y. F. Thiacalix[4]arene-functionalized molecular clusters

involving the Keggin-type PM_4Mo_8 (M= Co, Ni) motif: Electrochemical and photothermal conversion properties. *Polyoxometalates* **2025**, *4*, 9140091.
[32] Mato, M.; Rivas-Saborido, A.; Casas-Pais, A.; Tomás-Gamasa, M.; Mascareñas, J. L. Photoredox unmasking of aromatic C–H bonds in living environments enabled by thianthrenium salts. *J. Am. Chem. Soc.* **2026**, *148*, 5946–5952.
[33] Baek, J. W.; Goo, B. S.; Ahn, H.; Han, S.; Han, S. W. Merger of heterogeneous and homogeneous photocatalysis for arene C–H amination. *J. Am. Chem. Soc.* **2026**, *148*, 10806–10815.
[34] Ravelli, D.; Fagnoni, M.; Fukuyama, T.; Nishikawa, T.; Ryu, I. Site-selective C–H functionalization by decatungstate anion photocatalysis: Synergistic control by polar and steric effects expands the reaction scope. *ACS Catal.* **2018**, *8*, 701–713.
[35] Cybularczyk-Cecotka, M.; Predygier, J.; Crespi, S.; Szczepanik, J.; Giedyk, M. Photocatalysis in aqueous micellar media enables divergent C–H arylation and *N*-dealkylation of benzamides. *ACS Catal.* **2022**, *12*, 3543–3549.
[36] Senaweera, S.; Weaver, J. D. Dual C–F, C–H functionalization via photocatalysis: Access to multifluorinated biaryls. *J. Am. Chem. Soc.* **2016**, *138*, 2520–2523.
[37] Lai, X. L.; Shu, X. M.; Song, J. S.; Xu, H. C. Electrophotocatalytic decarboxylative C–H functionalization of heteroarenes. *Angew. Chem.* **2020**, *132*, 10713–10719.
[38] Wang, H.; Zhang, D.; Bolm, C. Sulfoximidations of benzylic C–H bonds by photocatalysis. *Angew. Chem., Int. Ed.* **2018**, *57*, 5863–5866.
[39] Niu, L. B.; Liu, J. M.; Liang, X. A.; Wang, S. C.; Lei, A. W. Visible light-induced direct α C–H functionalization of alcohols. *Nat. Commun.* **2019**, *10*, 467.
[40] Zhang, W. Y.; Burek, B. O.; Fernández-Fueyo, E.; Alcalde, M.; Bloh, J. Z.; Hollmann, F. Selective activation of C–H bonds in a cascade process combining photochemistry and biocatalysis. *Angew. Chem., Int. Ed.* **2017**, *56*, 15451–15455.
[41] Xu, S. Y.; Wang, P.; Zhang, B. W.; Wang, C.; Low, J.; Ivanov, V. K.; Zhang, Z. M. Nickel-substituted polyoxometalate-CdS single-cluster photocatalysts for efficient plastic waste degradation coupled with H_2 production. *Polyoxometalates* **2025**, *4*, 9140096.
[42] Wu, X. J.; Xie, S. J.; Vangestel, D.; Zhao, H.; Sels, B. Green solvent γ-valerolactone (GVL) facilitates photocatalytic C–H bond activation. *Angew. Chem.* **2024**, *136*, e202409826.
[43] Dong, H.; Zhang, X.; Yan, X. C.; Wang, Y. X.; Sun, X. J.; Zhang, G. L.; Feng, Y. J.; Zhang, F. M. Mixed-metal-cluster strategy for boosting electrocatalytic oxygen evolution reaction of robust metal-organic frameworks. *ACS Appl. Mater. Interfaces* **2019**, *11*, 45080–45086.
[44] Jiao, J. C.; Zhang, L.; Hu, H. N.; Sun, H.; Xu, Z. Q.; Pu, Y. F.; Han, Q. X. Designing a polyoxometalate-pillared metal-organic framework with long-range delocalization *for* photocatalytic oxidative cross-coupling. *J. Catal.* **2025**, *450*, 116309.
[45] Simms, C.; Mullaliu, A.; Sarson, E. T.; Solé-Daura, A.; Puiggalí-Jou, J.; Carbó, J. J.; Aquilanti, G.; Parac-Vogt, T. N. Tuning oxygen occupancy within metal-oxo clusters for enhancing catalytic activity of Zr-MOFs. *ACS Catal.* **2025**, *15*, 14279–14292.
[46] Marcano, D. E. S.; Savić, N. D.; Declerck, K.; Abdelhameed, S. A. M.; Parac-Vogt, T. N. Reactivity of metal-oxo clusters towards biomolecules: From discrete polyoxometalates to metal-organic frameworks. *Chem. Soc. Rev.* **2024**, *53*, 84–136.
[47] Li, J.; Liu, X. L.; Zheng, J.; Li, F.; Chen, Y. H.; Han, Q. X. A tailored polyoxometalate-based metal-organic framework: Boosting photocatalytic Knoevenagel condensation through efficient proton and hydrogen atom transfer. *J. Catal.* **2025**, *452*, 116416.
[48] Zhang, B. C.; Cao, X. C.; Wen, J.; Guo, S. H.; Duan, X. C.; Zhang, X. M. Integration of Plasmonic materials with MOFs/MOF-derived materials for Photocatalysis. *Coord. Chem. Rev.* **2024**, *518*, 216113.
[49] Doan, T. D.; Vu, N. N.; Hoang, T. L. G.; Nguyen-Tri, P. Metal-organic framework (MOF)-based materials for photocatalytic antibacterial applications. *Coord. Chem. Rev.* **2025**, *523*, 216298.
[50] Zhao, J. D.; Ren, G. M.; Meng, X. C. Recent advances on MOFs for photocatalytic and electrocatalytic nitrogen reduction to produce ammonia. *Nano Energy* **2024**, *130*, 110109.
[51] Biserčić, M. S.; Marjanović, B.; Zasońska, B. A.; Stojadinović, S.; Ćirić-Marjanović, G. Novel microporous composites of MOF-5 and polyaniline with high specific surface area. *Synthetic. Met.* **2020**, *262*, 116348.
[52] Hu, L.; Wu, W.; Hu, M.; Jiang, L.; Lin, D.; Wu, J.; Yang, K. Double-walled Al-based MOF with large microporous specific surface area for trace benzene adsorption. *Nat. Commun.* **2024**, *15*, 3204.
[53] Liu, R. L.; Chen, Y. F.; Su, X.; Zhu, W. P.; Liu, Z. C.; Chen, Y. H.; Wang, D. Y.; Li, G. Proton conductive polyoxometalates. *Coord. Chem. Rev.* **2025**, *522*, 216224.
[54] Ebrahimi, A.; Krivosudský, L.; Cherevan, A.; Eder, D. Polyoxometalate-based porphyrinic metal-organic frameworks as heterogeneous catalysts. *Coord. Chem. Rev.* **2024**, *508*, 215764.
[55] Boskovic, C. Rare earth polyoxometalates. *Acc. Chem. Res.* **2017**, *50*, 2205–2214.
[56] Zhang, Z. M.; Zhang, T.; Wang, C.; Lin, Z. K.; Long, L. S.; Lin, W. B. Photosensitizing metal-organic framework enabling visible-light-driven proton reduction by a wells-Dawson-type polyoxometalate. *J. Am. Chem. Soc.* **2015**, *137*, 3197–3200.
[57] Weinstock, I. A.; Schreiber, R. E.; Neumann, R. Dioxygen in polyoxometalate mediated reactions. *Chem. Rev.* **2018**, *118*, 2680–2717.
[58] Nandy, A.; Murmu, G.; Rana, A.; Saha, S.; Banerjee, S. Sprayed microdroplets architect a polyoxometalate framework. *Angew. Chem.* **2025**, *137*, e202424745.
[59] Liu, J. X.; Zhang, X. B.; Li, Y. L.; Huang, S. L.; Yang, G. Y. Polyoxometalate functionalized architectures. *Coord. Chem. Rev.* **2020**, *414*, 213260.
[60] Li, H. Y.; Zheng, L. R.; Lu, Q. C.; Li, Z.; Wang, X. A monolayer crystalline covalent network of polyoxometalate clusters. *Sci. Adv.* **2023**, *9*, eadi6595.
[61] Liu, J. C.; Zhao, J. W.; Streb, C.; Song, Y. F. Recent advances on high-nuclear polyoxometalate clusters. *Coord. Chem. Rev.* **2022**, *471*, 214734.
[62] Martin, C.; Kastner, K.; Cameron, J. M.; Hampson, E.; Alves Fernandes, J.; Gibson, E. K.; Walsh, D. A.; Sans, V.; Newton, G. N. Redox-active hybrid polyoxometalate-stabilised gold nanoparticles. *Angew. Chem.* **2020**, *132*, 14437–14441.
[63] Ogiwara, N.; Iwano, T.; Ito, T.; Uchida, S. Proton conduction in ionic crystals based on polyoxometalates. *Coord. Chem. Rev.* **2022**, *462*, 214524.
[64] Li, B. L.; Xu, X. T.; Lv, Y. F.; Wu, Z. H.; He, L.; Song, Y. F. Polyoxometalates as potential artificial enzymes toward biological applications. *Small* **2024**, *20*, 2305539.
[65] Li, L.; Yu, Y. T.; Zhang, N. N.; Li, S. H.; Zeng, J. G.; Hua, Y.; Zhang, H. Polyoxometalate (POM)-based crystalline hybrid photochromic materials. *Coord. Chem. Rev.* **2024**, *500*, 215526.
[66] Si, C.; Liu, X. L.; Jiao, J. C.; Xu, J. J.; Ye, L. H.; Li, J.; Han, Q. X. Developing single ligand strategy for engineering a high-performance photocatalyst with the pore space partition and open-metal sites. *Appl. Catal. B: Environ. Energy* **2025**, *362*, 124687.
[67] Xu, X. B.; Chen, S. M.; Chen, Y. F.; Sun, H. Y.; Song, L.; He, W.; Wang, X. Polyoxometalate cluster-incorporated metal-organic framework hierarchical nanotubes. *Small* **2016**, *12*, 2982–2990.
[68] Pascual-Borràs, M.; Arca, E.; Yoshikawa, H.; Penfold, T.; Waddell, P. G.; Errington, R. J. Mechanochemical polyoxometalate super-reduction with lithium metal. *J. Am. Chem. Soc.* **2024**, *146*, 26485–26496.
[69] Zhang, Z.; Liu, Y. W.; Tian, H. R.; Li, X. H.; Liu, S. M.; Lu, Y.; Sun, Z. X.; Liu, T. B.; Liu, S. X. Polyoxometalate-based metal-organic framework fractal crystals. *Matter* **2020**, *2*, 250–260.
[70] Gumerova, N. I.; Rompel, A. Synthesis, structures and applications of electron-rich polyoxometalates. *Nat. Rev. Chem.* **2018**, *2*, 0112.

[71] Wang, J. Z.; Cao, C. S.; Wang, J. W.; Zhang, Y. Q.; Zhu, L. Y. Insights into highly efficient photodegradation of poly/perfluoroalkyl substances by In-MOF/BiOF heterojunctions: Built-in electric field and strong surface adsorption. *Appl. Catal. B: Environ.* **2022**, *304*, 121013.
[72] Li, X. F.; Zhu, Q. L. MOF-based materials for photo- and electrocatalytic CO_2 reduction. *EnergyChem* **2020**, *2*, 100033.
[73] Liu, Y. Q.; Xin, X.; Shi, Y. H.; Zhao, Z. F.; Tan, J. D.; Yang, D.; Jiang, Z. Y. Three-ligand Ti-MOFs for high-efficient photocatalytic H_2 evolution. *Chem. Eng. J.* **2024**, *482*, 149193.
[74] Li, L. X.; Lv, X. Y.; Jin, L. J.; Du, K. X.; Jiang, J. H.; Zhao, X. H.; Liang, H. J.; Guo, Y. M.; Wang, X. B. Facile synthesis of Sn-doped MOF-5 catalysts for efficient photocatalytic nitrogen fixation. *Appl. Catal. B: Environ. Energy* **2024**, *344*, 123586.
[75] Sepehrmansourie, H.; Alamgholiloo, H.; Pesyan, N. N.; Zolfigol, M. A. A MOF-on-MOF strategy to construct double Z-scheme heterojunction for high-performance photocatalytic degradation. *Appl. Catal. B: Environ.* **2023**, *321*, 122082.
[76] Shi, Y.; Yang, A. F.; Cao, C. S.; Zhao, B. Applications of MOFs: Recent advances in photocatalytic hydrogen production from water. *Coord. Chem. Rev.* **2019**, *390*, 50–75.
[77] Li, D. D.; Zhou, Q. X.; Hu, X. G.; Mu, L.; Zeng, H.; Luo, J. W. Environmental decomposition and remodeled phytotoxicity of framework-based nanomaterials. *J. Hazard. Mater.* **2022**, *422*, 126846.
[78] Govindaraju, S.; Arumugasamy, S. K.; Chellasamy, G.; Yun, K. Zn-MOF decorated bio activated carbon for photocatalytic degradation, oxygen evolution and reduction catalysis. *J. Hazard. Mater.* **2022**, *421*, 126720.
[79] Zhang, X. L.; Jiang, W.; Di, J. Rational design and application of MOF-based materials for photocatalytic CO_2 reduction. *Small* **2026**, *22*, e13278.
[80] Huang, T. Y.; Yang, H.; Xu, W. L.; Sun, Y. Y.; Pang, H. Research progress of MOF-based materials in photocatalytic reduction of CO_2 and N_2. *Chem Catal.* **2024**, *4*, 100929.
[81] King, T. A.; Kandemir, J. M.; Walsh, S. J.; Spring, D. R. Photocatalytic methods for amino acid modification. *Chem. Soc. Rev.* **2021**, *50*, 39–57.
[82] Wu, E. J.; Zhou, J. T.; Ren, D. M.; He, H. G.; Pan, J. Y.; Tang, C. Q.; Zhuang, X. P. Structural-interfacial engineering of MOF-functionalized aerogels for efficient photocatalytic reduction of Cr(VI). *J. Hazard. Mater.* **2025**, *495*, 139019.
[83] Wang, X. W.; Zhu, L. F.; Lv, Z. W.; Qi, Z. L.; Xu, Y.; Miao, T. F.; Fu, X. L.; Li, L. F. Coupled visible-light driven photocatalytic reactions over porphyrin-based MOF materials. *Chem. Eng. J.* **2022**, *442*, 136186.
[84] Xu, C. Y.; Pan, Y. T.; Wan, G.; Liu, H.; Wang, L.; Zhou, H.; Yu, S. H.; Jiang, H. L. Turning on visible-light photocatalytic C–H oxidation over metal-organic frameworks by introducing metal-to-cluster charge transfer. *J. Am. Chem. Soc.* **2019**, *141*, 19110–19117.
[85] Zhu, Y. P.; Yin, J.; Abou-Hamad, E.; Liu, X. K.; Chen, W.; Yao, T.; Mohammed, O. F.; Alshareef, H. N. Highly stable phosphonate-based MOFs with engineered bandgaps for efficient photocatalytic hydrogen production. *Adv. Mater.* **2020**, *32*, 1906368.
[86] Ji, G. F.; Zhao, L.; Tang, Y.; Liu, S. T.; Wang, Y. F.; He, C.; Duan, C. Y. Ultrathin 2D cerium-based metal-organic framework nanosheet that boosts selective oxidation of inert C(sp3)-H bond through multiphoton excitation. *Small* **2023,** *19*, 2300597.
[87] Ouyang, J.; Quan, Y. J. Metal-organic framework catalyzed hydrogen atom transfer for photocatalytic organic synthetic applications. *ChemCatChem* **2024**, *16*, e202400112.
[88] Ji, G. F.; Zhao, L.; Wang, Y. F.; Tang, Y.; He, C.; Liu, S. T.; Duan, C. Y. A binuclear cerium-based metal-organic framework as an artificial monooxygenase for the saturated hydrocarbon aerobic oxidation with high efficiency and high selectivity. *ACS Catal.* **2022**, *12*, 7821–7832.
[89] Schlachter, A.; Asselin, P.; Harvey, P. D. Porphyrin-containing MOFs and COFs as heterogeneous photosensitizers for singlet oxygen-based antimicrobial nanodevices. *ACS Appl. Mater. Interfaces* **2021**, *13*, 26651–26672.
[90] Karmakar, S.; Barman, S.; Rahimi, F. A.; Maji, T. K. Covalent grafting of molecular photosensitizer and catalyst on MOF-808: Effect of pore confinement toward visible light-driven CO_2 reduction in water. *Energy Environ. Sci.* **2021**, *14*, 2429–2440.
[91] Ma, Y.; Li, X. Y.; Li, A. J.; Yang, P.; Zhang, C. Y.; Tang, B. H_2S-activable MOF nanoparticle photosensitizer for effective photodynamic therapy against cancer with controllable singlet-oxygen release. *Angew. Chem., Int. Ed.* **2017**, *56*, 13752–13756.
[92] Wu, Y. A.; Guo, Y. J.; Feng, K. J.; Li, M.; Li, H. X.; Wu, J. S.; Wang, P. F.; Yang, R. G.; He, X.; Yin, X. et al. MOF-based hypocrellin composite nanomaterials as advanced plant-derived photosensitizers for multimodal therapy. *Chem. Eng. J.* **2025**, *520*, 166071.
[93] Rajasree, S. S.; Saha, B.; Kelly, G. M.; Phillips, E. N.; Maindan, K.; Li, A.; Slusarczyk, T.; Deria, P. Metal-organic framework-based efficient singlet heterogeneous photoredox catalyst for aerobic C–H functionalization. *ACS Catal.* **2025**, *15*, 3515–3524.
[94] Yu, Q. C.; Deng, Z. H.; Chen, R. D.; Zhang, J. Y.; Kwok, R. T. K.; Lam, J. W. Y.; Sun, J. W.; Tang, B. Z. Ligand-to-ligand charge transfer induced red-shifted room temperature phosphorescence in metal-organic frameworks. *J. Am. Chem. Soc.* **2025**, *147*, 10530–10539.
[95] Xu, W. J.; Huang, B. X.; Li, G. L.; Yang, F.; Lin, W.; Gu, J. X.; Deng, H. G.; Gu, Z. G.; Jin, H. G. Donor-acceptor mixed-naphthalene diimide-porphyrin MOF for boosting photocatalytic oxidative coupling of amines. *ACS Catal.* **2023**, *13*, 5723–5732.
[96] Jin, J. K.; Wu, K.; Liu, X. Y.; Huang, G. Q.; Huang, Y. L.; Luo, D.; Xie, M.; Zhao, Y. F.; Lu, W. G.; Zhou, X. P. et al. Building a pyrazole-benzothiadiazole-pyrazole photosensitizer into metal-organic frameworks for photocatalytic aerobic oxidation. *J. Am. Chem. Soc.* **2021**, *143*, 21340–21349.
[97] Ding, C. W.; Luo, W. Z.; Zhou, J. Y.; Ma, X. J.; Chen, G. H.; Zhou, X. P.; Li, D. Hydroxo iron(III) sites in a metal-organic framework: Proton-coupled electron transfer and catalytic oxidation of alcohol with molecular oxygen. *ACS Appl. Mater. Interfaces* **2019**, *11*, 45621–45628.
[98] Gao, H.; Tang, Y.; Liu, S. T.; He, C.; Li, H. Q.; Zhao, L.; Duan, C. Y. Eosin Y post-decorated metal-organic framework as a selectivity regulator for the alcohols oxidation. *ACS Appl. Mater. Interfaces* **2024**, *16*, 37896–37905.
[99] Wang, Z. H.; Zeng, L.; He, C.; Duan, C. Y. Photocatalytic C–H activation with alcohol as a hydrogen atom transfer agent in a 9-fluorenone based metal-organic framework. *ACS Appl. Mater. Interfaces* **2021**, *13*, 25898–25905.
[100] Ran, L.; Feng, N.; Dong, Y. M.; Cai, H. Y.; Chen, Y. P.; Teng, H. L. Rational design of MOF-based multifunctional bio-nanoreactor for efficient detection and photo-degradation of chloramphenicol. *Adv. Sci.* **2025**, *12*, 2414866.
[101] Jia, X. C.; Li, H. Y.; Gao, Y.; Zhang, Y. H.; Yang, C.; Jiao, Y.; Duan, C. Y. Modulation of MOF energy state to construct smart activated sensitizers for membrane directed C–H ketene therapy in tumor cells. *Adv. Mater.* **2026**, *38*, e19153.
[102] Yan, B. Photofunctional MOF-based hybrid materials for the chemical sensing of biomarkers. *J. Mater. Chem. C* **2019**, *7*, 8155–8175.
[103] Feng, B.; Feng, D. N.; Wan, K.; Pei, Y.; Zong, B. N.; Li, H. X.; Li, W.; Qiao, M. H. Defective MOFs microreactor with heterojunction for selective methane photocatalysis via desorption-driven overoxidation suppression. *Adv. Sci.* **2026**, *13*, e13507.
[104] Li, B.; Yu, X. L.; Wang, J. J.; Tang, H.; Sun, X. S.; Cheng, L. J.; Zhou, H. P.; Tian, Y. P.; Li, D. D. Unlocking efficient high-order multiphoton-excited fluorescence of metal-organic framework via

octupolar module *in situ* formation. *Adv. Funct. Mater.* **2023**, *33*, 2305391.

[105] Ghosh, A.; Surendran, D.; Barman, S.; Jena, R.; Bhakar, M.; Nath, S.; Sheet, G.; Zaręba, J. K.; Maji, T. K. Photo-piezocatalytic water splitting by post-synthetic charge-transfer complexation driven cluster modification in Ce-based MOF-808. *Adv. Mater.* **2026**, *38*, e11679.

[106] Youssef, A.; Telegeiev, I.; Dhainy, J.; Alboudone, N.; Lebedev, O. I.; El Fallah, J.; Hmadeh, M.; El-Roz, M. Poly-single-atom photocatalysts on UiO-66 scaffolds for superior CO_2 conversion under visible light. *ACS Appl. Mater. Interfaces* **2025**, *17*, 32248–32259.

[107] Zhang, T.; Jiao, J. C.; Guo, K. X.; Zhang, L.; Xu, J. J.; Han, Q. X. Tailoring a decatungstate-incorporated metal-organic framework for light-driven [3+2] cyclization of phenols with olefins. *J. Catal.* **2024**, *436*, 115637.

[108] Lv, Y. J.; Peng, D. X.; Zhang, W. X.; Sun, J.; Sun, H. Y.; Wang, X.; Li, X.; Ma, M. W.; Su, Z. M. Visible-light-mediated oxidation of saturated C(sp^3)-H bonds over $[W_{10}O_{32}]^{4-}$-POMOFs. *J. Catal.* **2025**, *446*, 116088.

[109] Ma, P.; Ding, M. L.; Rong, W.; Liu, X.; Yao, J. F. Acetic acid-assisted polyhydroxy acid modification of a zirconium-based MOF for synergistic CO_2 fixation. *J. Environ. Chem. Eng.* **2022**, *10*, 108739.

[110] Jiao, J. C.; Zhang, C. B.; Sun, H.; Hu, H. N.; Xu, Z. Q.; Zhao, J. W.; Han, Q. X.; Ma, P. T. Photocatalytic oxidation of various C–H bonds by a polyoxometalate nanocluster-dominated compartmentalized metal-organic framework. *Green Chem.* **2025**, *27*, 7608–7619.

[111] Sun, C. Y.; Liu, S. X.; Liang, D. D.; Shao, K. Z.; Ren, Y. H.; Su, Z. M. Highly stable crystalline catalysts based on a microporous metal-organic framework and polyoxometalates. *J. Am. Chem. Soc.* **2009**, *131*, 1883–1888.

[112] Buru, C. T.; Li, P.; Mehdi, B. L.; Dohnalkova, A.; Platero-Prats, A. E.; Browning, N. D.; Chapman, K. W.; Hupp, J. T.; Farha, O. K. Adsorption of a catalytically accessible polyoxometalate in a mesoporous channel-type metal-organic framework. *Chem. Mater.* **2017**, *29*, 5174–5181.

[113] Shen, Q. B.; Chen, J. L.; Jing, X.; Duan, C. Y. Polyoxometalate-embedded metal-organic framework as an efficient copper-based monooxygenase for C(sp^3)-H bond oxidation via multiphoton excitation. *ACS Catal.* **2023**, *13*, 9969–9978.

[114] Rana, M.; AL-Fayaad, H. A.; Luo, B.; Lin, T.; Ran, L. B.; Clegg, J. K.; Gentle, I.; Knibbe, R. Oriented nanoporous MOFs to mitigate polysulfides migration in lithium-sulfur batteries. *Nano Energy* **2020**, *75*, 105009.

[115] Alrayyes, A. U.; Boga, K.; Wang, H. T.; Saito, K. Construction of a MOF/polysiloxane-based nanocomposite membrane with precise gas separation phototuning. *ACS Appl. Polym. Mater.* **2024**, *6*, 13567–13573.

[116] Xin, Q. P.; Dong, J. K.; Shao, W.; Ding, X. L.; Gao, N. N.; Zhang, L.; Jin, H. M.; Chen, H.; Zhang, Y. Z. Reversible MOF-based mixed matrix membranes for SO_2/N_2 separation: A photo-responsive approach. *J. Membr. Sci.* **2025**, *714*, 123431.

[117] Li, P. Y.; Wang, X. Y.; Wang, D. J.; Xie, T. F.; Lin, Y. H. Interface built-in electric field regulation in Co_5Mn_{12}-MOF/Ti-Fe_2O_3: Boosting photocarrier separation for high-efficiency photo-assisted Zn-air batteries. *Mater. Today Energy* **2026**, *57*, 102231.

[118] Ma, Y. Y.; Li, L.; Jiang, Y. F.; Wang, Z. B.; Wang, B.; Zhang, W. M. Promoting photon-generated carrier separation via a type-II Cu_2O@MOF heterojunction cathode for photo-rechargeable zinc-ion batteries. *J. Colloid Interface Sci.* **2026**, *709*, 139949.

[119] Li, X. X.; Hong, X. X.; Liao, Z. Y.; Zhang, L.; Li, R. H.; Zeng, Y.; Liu, Y.; Li, S. L.; Lan, Y. Q. Tri-functional molecular junction photocatalyst for cascade synthesis of N-benzylideneaniline derivatives. *Sci. Bull.* **2024**, *69*, 3661–3665.

[120] Amtawong, J.; Skjelstad, B. B.; Handford, R. C.; Suslick, B. A.; Balcells, D.; Tilley, T. D. C–H activation by $RuCo_3O_4$ oxo cubanes: Effects of oxyl radical character and metal-metal cooperativity. *J. Am. Chem. Soc.* **2021**, *143*, 12108–12119.

[121] Jana, S.; Pattanayak, S.; Das, S.; Ghosh, M.; Velasco, L.; Moonshiram, D.; Gupta, S. S. Comparing the reactivity of an oxoiron(IV) cation radical and its oxoiron(V) tautomer towards C–H bonds. *Chem. Commun.* **2023**, *59*, 2755–2758.

[122] Itabashi, Y.; Asahara, H.; Ohkubo, K. Chlorine-radical-mediated C–H oxygenation reaction under light irradiation. *Chem. Commun.* **2023**, *59*, 7506–7517.

[123] Lu, Z. P.; Ju, M.; Wang, Y.; Meinhardt, J. M.; Martinez Alvarado, J. I.; Villemure, E.; Terrett, J. A.; Lin, S. Regioselective aliphatic C–H functionalization using frustrated radical pairs. *Nature* **2023**, *619*, 514–520.

[124] Zhao, L.; Cai, W.; Ji, G. F.; Wei, J. W.; Du, Z. G.; He, C.; Duan, C. Y. Anthraquinone-based metal-organic frameworks as a bifunctional photocatalyst for C–H activation. *Inorg. Chem.* **2022**, *61*, 9493–9503.

[125] Cheng, Y.; Shi, W. X.; Zhang, Z. M. Decatungstate-doped Ce-MOF for methane photooxidation. *Chin. Chem. Lett.* **2025**, *36*, 110387.

[126] Wang, L.; Li, S. R.; Chen, Y. Z.; Jiang, H. L. Encapsulating copper nanocrystals into metal-organic frameworks for cascade reactions by photothermal catalysis. *Small* **2021**, *17*, 2004481.

[127] Wang, X. S.; Fan, G. L.; Guo, S. J.; Gao, R.; Guo, Y.; Han, C. H.; Gao, Y. L.; Zhang, J. W.; Gu, X. J.; Wu, L. M. Regulated dual defects of bridging organic and terminal inorganic ligands in iron-based metal-organic framework nodes for efficient photocatalytic ammonia synthesis. *Angew. Chem.* **2024**, *136*, e202404258.

[128] Golden, D. L.; Zhang, C. F.; Chen, S. J.; Vasilopoulos, A.; Guzei, I. A.; Stahl, S. S. Benzylic C–H esterification with limiting C–H substrate enabled by photochemical redox buffering of the Cu catalyst. *J. Am. Chem. Soc.* **2023**, *145*, 9434–9440.

[129] Xi, Y. F.; Gao, R. X.; Fang, P.; Han, Y. P.; Ma, C.; Mei, T. S. Site-selective benzylic C–H oxidation through mediated electrolysis. *Chin. J. Catal.* **2024**, *67*, 54–60.

[130] Zheng, Y. Y.; Shen, Q. B.; Li, Z. T.; Jing, X.; Duan, C. Y. Two copper-containing polyoxometalate-based metal-organic complexes as heterogeneous catalysts for the C–H bond oxidation of benzylic compounds and olefin epoxidation. *Inorg. Chem.* **2022**, *61*, 11156–11164.

[131] An, Z. X.; Zhang, Z.; Li, X. H.; Wang, X. L. Wells-dawson-type polyoxometalate-based copper complexes with dual catalytic active sites for highly selective oxidation of alkylbenzene C–H bonds. *Inorg. Chem.* **2025**, *64*, 17379–17386.

[132] Kim, Y. L.; Park, S. A.; Choi, S. M.; Park, J. U.; Kim, J. H. Co^{III}-catalyzed C–H alkenylation and allylation with cyclopropenes via sequential C–H/C–C bond activation. *Org. Lett.* **2021**, *23*, 6674–6679.

[133] Massignan, L.; Zhu, C. J.; Hou, X. Y.; Oliveira, J. C. A.; Salamé, A.; Ackermann, L. Manganaelectro-catalyzed azine C–H arylations and C–H alkylations by assistance of weakly coordinating amides. *ACS Catal.* **2021**, *11*, 11639–11649.

[134] Shi, D. Y.; Wang, S. J.; Cui, C. J.; Zhou, Q.; Du, J. P.; Chen, D. M. A decatungstate incorporated MOF for visible-light-driven photocatalytic oxidation of cyclohexane by molecular oxygen. *J. Clust. Sci.* **2021**, *32*, 579–584.

[135] Wan, H. T.; Tan, C. L.; Qi, M. Y.; Wang, Y. F.; Tang, Z. R.; Xu, Y. J. Efficient methane to ethane conversion via C–H bond activation catalyzed by a MOF-derived porous PdO/TiO_2 nanocomposite. *Nanoscale Horiz.* **2026**, *11*, 283–288.

[136] Li, M. L.; Kwong, F. Y. Cobalt-catalyzed tandem C–H activation/C–C cleavage/C–H cyclization of aromatic amides with alkylidenecyclopropanes. *Angew. Chem.* **2018**, *130*, 6622–6626.

Yanjie Lv is a female doctoral student admitted in 2024. She is currently pursuing her doctoral degree at the College of Chemistry and Environmental Engineering, Changchun University of Science and Technology. Her research concentrates on the structural design and synthesis of multi-sulfonate-based metal-organic frameworks, as well as the exploration of their photocatalytic performance. Her research system regulates metal species, coordination modes and structural dimensions to realize targeted material synthesis. She further investigates the applications of these materials in C–H bond oxidation reactions. She has published several SCI-indexed academic papers in international journals, including *Journal of Catalysis*, *Chinese Chemical Letters*, and *Polyoxometalates*.

Jing Sun is a professor and doctoral supervisor and serves as Director of the Jilin Provincial Center for Innovation in Optical Materials and Chemical Technology. She is a member of the Jilin Provincial Professional Degree Graduate Education Guidance Committee. She acts as a member of the 7th Rare Earth Crystal Professional Committee under the Chinese Rare Earth Society. She also holds the post of standing council member of the Jilin Chemical Society. Her primary research interests focus on optofunctional materials and chemistry. She has presided over or participated in more than 20 research projects, among which three research projects are currently in progress. She finished one academic monograph as the first author. She has obtained two authorized Chinese invention patents. She has published over 50 SCI-indexed papers in authoritative journals including *Analytical Chemistry*, *Coordination Chemistry Reviews*, *Chemical Engineering Journal*, *Journal of Colloid and Interface Science*, and *Journal of Catalysis*. One of her published papers has been selected as both a highly cited paper and a hot paper. She won the ICF Outstanding Paper Award during 2014–2023. She was awarded the Third Prize of Jilin Provincial Natural Science Award with the first ranking.

Xiao Li is an Associate Professor and Master's supervisor of Changchun University of Science and Technology, China. She holds the position of Department Chair of the School of Chemistry and Environmental Engineering. Her long-term research focuses on the synthesis of metal-organic framework (MOF) materials and polyoxometalate (POM)-based composite materials as well as their functional applications. Her research mainly contains two directions. The first direction covers carbon-coated multicomponent materials derived from bimetallic metal-organic frameworks and polyoxometalate@metal-organic framework composites toward electrocatalytic water splitting. The second direction involves the synthesis of multifunctional metal-organic frameworks and their composite materials, together with investigations on their performance in dye degradation, fluorescence sensing and ion adsorption. In recent years, she has published more than ten SCI-indexed papers as the first author or corresponding author, including *Advanced Functional Materials*, *Chemical Engineering Journal*, *Journal of Catalysis*, *Chinese Chemical Letters, Polyoxometalates*, *Inorganic Chemistry*, *Dyes and Pigments*, and *International Journal of Hydrogen Energy*.

Zhongmin Su is a Distinguished Professor and doctoral supervisor at Jilin University, a Tang Aoqing Scholar, a First-Class Professor of Jilin Province, and a national specially appointed high-end talent professor. He was honored as One of the Outstanding Talents across the Century by the Ministry of Education. He served as a member of the Chemistry Discipline Evaluation Group of the State Council Academic Degrees Committee for the sixth and seventh terms. He is a National Outstanding Backbone Teacher of Institutions of Higher Education. He has been awarded the National May 1st Labor Medal issued by the All-China Federation of Trade Unions and the honorary title of Special-Class Model Worker of Changchun City. His research interests cover theoretical and computational chemistry combining experimental and theoretical research strategies, together with functional materials chemistry. In recent years, he has published 285 SCI-indexed research papers in high-profile journals including Journal of the American Chemical Society, Angewandte Chemie International Edition and Nature Communications. He has won the Second Prize of the National Natural Science Award, as well as the First Prize of Natural Science Award and the First Prize of Science and Technology Progress Award of Jilin Province. He was selected as a Clarivate Analytics Global Highly Cited Researcher during 2014–2018 and in 2022. He was included in Elsevier's list of China Most Cited Researchers from 2016 to 2025. According to the ScholarGPS 2024 ranking, he ranks among the top 0.05% of scientists worldwide in the lifetime academic ranking. He presided over the Innovative Team Project supported by the Changjiang Scholars Program of the Ministry of Education. He acted as the principal investigator for multiple key research projects, such as the predictive project of the National 973 Program, research projects of the National 863 Program and key programs funded by the National Natural Science Foundation of China. He once held multiple part-time academic and administrative posts, including Part-time Vice Chairman of Jilin Provincial Association for Science and Technology, Council Member of the Chinese Chemical Society, and Vice President of Jilin Chemical Society. He previously worked as the Director of Jilin Provincial Center for Optical Materials, Chemical Science and Technology Innovation. He has undertaken important administrative positions including Deputy Director of Jilin Provincial Department of Education, Vice President of Northeast Normal University, and President of Changchun University of Science and Technology. At present, he acts as an Advisory Editorial Board Member of the journal Polyoxometalates. He serves as the Chair of the Sixth Council of Jilin Provincial Education Foundation. He also holds the position of Deputy Chair of the Academic Committee of Jilin University